

Electronic, vibrational, and torsional couplings in *N*-methylpyrrole: Ground, first excited, and cation states

Cite as: J. Chem. Phys. 154, 224305 (2021); <https://doi.org/10.1063/5.0050654>

Submitted: 17 March 2021 . Accepted: 12 May 2021 . Published Online: 10 June 2021

Alexander R. Davies, David J. Kemp, and  Timothy G. Wright



View Online



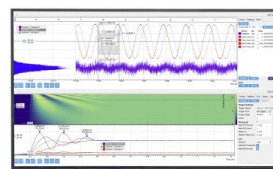
Export Citation



CrossMark

Challenge us.

What are your needs for
periodic signal detection?



Zurich
Instruments

Electronic, vibrational, and torsional couplings in *N*-methylpyrrole: Ground, first excited, and cation states

Cite as: J. Chem. Phys. 154, 224305 (2021); doi: 10.1063/5.0050654

Submitted: 17 March 2021 • Accepted: 12 May 2021 •

Published Online: 10 June 2021



View Online



Export Citation



CrossMark

Alexander R. Davies, David J. Kemp, and Timothy G. Wright^{a)} 

AFFILIATIONS

School of Chemistry, University of Nottingham, University Park, Nottingham NG7 2RD, United Kingdom

^{a)} Author to whom correspondence should be addressed: Tim.Wright@nottingham.ac.uk

ABSTRACT

The electronic spectrum associated with the $S_1 \leftarrow S_0 (\bar{A}^1 A_2 \leftarrow \bar{X}^1 A_1)$ one-photon transition of jet-cooled *N*-methylpyrrole is investigated using laser-induced fluorescence (LIF) and (1 + 1) resonance-enhanced multiphoton ionization (REMPI) spectroscopy; in addition, the (2 + 2) REMPI spectrum is considered. Assignment of the observed bands is achieved using a combination of dispersed fluorescence (DF), two-dimensional LIF (2D-LIF), zero-electron-kinetic energy (ZEKE) spectroscopy, and quantum chemical calculations. The spectroscopic studies project the levels of the S_1 state onto those of either the S_0 state, in DF and 2D-LIF spectroscopy, or the ground state cation (D_0^+) state, in ZEKE spectroscopy. The assignments of the spectra provide information on the vibrational, vibration-torsion (vibtor), and torsional levels in those states and those of the S_1 levels. The spectra are indicative of vibronic (including torsional) interactions between the S_1 state and other excited electronic states, deduced both in terms of the vibrational activity observed and shifts from expected vibrational wavenumbers in the S_1 state, attributed to the resulting altered shape of the S_1 surface. Many of the ZEKE spectra are consistent with the largely Rydberg nature of the S_1 state near the Franck–Condon region; however, there is also some activity that is less straightforward to explain. Comments are made regarding the photodynamics of the S_1 state.

© 2021 Author(s). All article content, except where otherwise noted, is licensed under a Creative Commons Attribution (CC BY) license (<http://creativecommons.org/licenses/by/4.0/>). <https://doi.org/10.1063/5.0050654>

I. INTRODUCTION

Pyrroles, including *N*-methylpyrroles, are key building blocks of many biomolecules (e.g., tryptophan, haem B, melatonin, and phycobiliproteins), a range of medicines (including photomedicines),^{1,2} metalloporphyrin-based metal–organic frameworks (MOFs),³ and molecular wires.⁴ *N*-methylpyrrole (NMP) has been the subject of a number of photodissociation studies,^{5–11} which have compared and contrasted its behavior with that of pyrrole.¹² A detailed understanding of the photophysics and photodynamics of molecules relies on establishing the energy-level structure; as such, there have been a number of spectroscopic studies of NMP.

The absorption spectrum of gaseous NMP molecules at ambient temperature has been reported by Milazzo,¹³ McDiarmid and Xing,¹⁴ and Cooper *et al.*¹⁵ Spectra of supersonic-jet-cooled molecules have been presented by McDiarmid and Xing,¹⁴ Philis,^{16,17} and Biswas *et al.*¹⁸ additionally, suggested

assignments of the S_1 vibrational and torsional levels were given by Woo and Kim.¹¹ A theoretical study of the torsional levels in NMP was published by Kanamaru,¹⁹ although we have questioned some of the conclusions of that work.²⁰

The low-lying electronic states of pyrrole and NMP are interesting, with occupied orbitals that are mixtures of valence and Rydberg character; for pyrrole and other molecules, the ramifications of such Rydberg-valence character on photodynamics have been discussed by Paterson and Townsend.²¹

Initially, treating the methyl group as a point mass, the point group symmetry of NMP is C_{2v} . Here, we locate the pyrrolyl ring in the *yz*-plane, with the N–CH₃ bond lying along the *z*-axis. The ground electronic state configuration may then be written as $\dots a_1^2 b_1^2 a_2^2$, where the a_1 symmetry orbital is mainly σ bonding (N–CH₃) and the two outermost occupied orbitals are π bonding. At the S_0 optimized geometry, the lowest-lying unoccupied orbitals are largely Rydberg-like and are accessed following vertical excitation

from the two outermost occupied orbitals into these. The symmetry of the lowest Rydberg states are $3s$ (a_1), $3p_x$ (b_1), $3p_y$ (b_2), and $3p_z$ (a_1). We shall come back to these later, but here we note that the lowest-energy vertical excitation is the $3s \leftarrow a_2$ excitation, yielding the $S_1^1A_2$ first excited state. In addition, the highest occupied orbital in the S_1 state evolves from $3s$ character in the Franck-Condon region to σ^* character at extended N-CH₃ bond lengths.⁹ Accessing this state is electronically forbidden in a one-photon transition,²² although it has been seen in two-photon transitions in some of the above-cited work^{11,14-16} and herein; as such, the activity seen in the one-photon spectrum arises from vibronic interactions. We shall consider both the one- and two-photon $\tilde{A} \leftarrow \tilde{X}$ spectra of NMP in the present work.

The main focus here will be the vibrational and vibration-torsional (vibtor) levels in the S_0 , S_1 , and D_0^+ electronic states of NMP, building on our earlier two-dimensional LIF (2D-LIF) and zero-electron-kinetic energy (ZEKE) study that concentrated on the torsional levels²⁰ and where we reported the adiabatic ionization energy (AIE) as $64\,250 \pm 5$ cm⁻¹. Here, we extend the earlier spectroscopic work to provide more definitive assignments of the S_1 levels, via both fluorescence and ZEKE spectroscopies. The latter allows vibrational wavenumbers for ground electronic state NMP⁺ to be established for the first time. In addition, we obtain gas-phase S_0 vibrational wavenumbers, a number for the first time, from the dispersed fluorescence (DF) and 2D-LIF spectra; these values are largely similar to liquid-/solution-phase IR and Raman values.²³⁻²⁵ By comparing the results of quantum chemical calculations for the S_1 and D_0^+ states with experimental vibrational wavenumbers, it is concluded that the shape of the S_1 potential energy surface is modified by the vibronic interactions, particularly along out-of-plane coordinates.

II. EXPERIMENTAL

The REMPI/ZEKE²⁶ and 2D-LIF²⁷ apparatuses are the same as those employed earlier and in the recent study addressing the torsional levels in NMP and NMP⁺.²⁰ In all of the present experiments, a free-jet expansion of the vapor above room-temperature NMP liquid (Sigma-Aldrich, 99% purity) seeded in 2 bars Ar was employed.

For the fluorescence experiments, the free-jet expansion was intersected at $X/D \sim 20$ by the frequency-doubled output of a single dye laser (Sirah CobraStretch), operating with Coumarin 480 and pumped with the third harmonic of a Surelite III Nd:YAG laser. For the LIF spectra, the fluorescence was focused onto a photomultiplier tube (Hamamatsu H10721-01). For the 2D-LIF spectra, the fluorescence was collected, collimated, and focused onto the entrance slits of a 1.5 m Czerny-Turner spectrometer (Sciencetech 9150) operating in single-pass mode, dispersed by a 3600 groove/mm grating, allowing ~ 380 cm⁻¹ windows of the dispersed fluorescence to be collected by a CCD camera (Andor iStar DH334T). At a fixed grating angle of the spectrometer, the excitation laser was scanned, and at each excitation wavenumber, the camera image was accumulated for 2000 laser shots. This allowed a plot to be produced of fluorescence intensity vs both the excitation laser wavenumber and the wavenumber of the emitted and dispersed fluorescence, termed a 2D-LIF spectrum.^{28,29}

For the ZEKE spectra of NMP, the focused outputs of two dye lasers (Sirah CobraStretch) were overlapped spatially and temporally and passed through a vacuum chamber coaxially and counterpropagating, where they intersected the free-jet expansion. The excitation laser operated with Coumarin 480 and was pumped with the third harmonic (355 nm) of a Surelite III Nd:YAG laser. The fundamental of the excitation laser was used to record the (2 + 2) REMPI spectrum, while for the (1 + 1) REMPI and the ZEKE spectra, that output was frequency doubled. In the ZEKE experiments, the ionization laser operated with Coumarin 440, pumped with the third harmonic (355 nm) of a Surelite I Nd:YAG laser, and the output was undoubled. The jet expansion passed between two biased electrical grids located in the extraction region of a time-of-flight mass spectrometer, which was employed in the REMPI experiments. These grids were also used in the ZEKE experiments by application of pulsed voltages, giving typical fields of ~ 10 V cm⁻¹, after a delay of ~ 2 μ s; this delay was minimized while avoiding the introduction of excess noise from the prompt electron signal. The resulting ZEKE bands had widths of ~ 5 – 7 cm⁻¹. Electron and ion signals were recorded on separate sets of microchannel plates.

We also report photoionization efficiency (PIE) curves for some selected levels, where we fix the excitation laser on a particular S_1 level and then scan the ionization laser across the ionization threshold, recording the NMP⁺ ion yield. The PIE curves were recorded with the same setup used for the REMPI experiments.

III. RESULTS AND DISCUSSION

A. Nomenclature

1. Electronic states

Generally, we shall refer to electronic and vibrational symmetries using C_{2v} point group symmetry labels. When we consider torsional and vibration-torsion (vibtor) levels, we shall employ G_{12} molecular symmetry group (MSG) labels.³⁰ In Table I, we give the correspondence between these two sets of labels. Both the symmetry labels employed will be clear from the context since the G_{12} labels have prime (') or double prime (") embellishments, while the C_{2v} labels do not; occasionally, we give both the C_{2v} and G_{12} symmetry labels to aid the reader.

TABLE I. Correspondence of the C_{2v} point group symmetry classes with those of the G_{12} molecular symmetry group. Also indicated are the symmetries of the P_i vibrations and the pure torsional levels.^a

C_{2v}	G_{12}	P_i^b	m
a_1	a_1'	P_{1-9}	0, 6(+)
a_2	a_2'	P_{10-12}	6(-)
b_1	a_2''	P_{13-16}	3(-)
b_2	a_1''	P_{17-24}	3(+)
	e'		2, 4
	e''		1, 5

^aSymmetries of vibtor levels can be obtained by combining the vibrational symmetry (in G_{12}) with those of the pure torsional level using a D_{3h} point group direct product table.

^bThe P_i vibrational labels are described in Ref. 33, where mode diagrams may also be found.

The ground electronic state, S_0 , of NMP is \tilde{X}^1A_1 and, as given above, has an outermost electronic configuration $\dots a_1^2 b_1^2 a_2^2$. The lowest energy unoccupied orbitals in the Franck–Condon (FC) region, which are of interest to the present work, are largely Rydberg in character, corresponding to the $3s$ or $3p_{x,y,z}$ orbitals. The first electronically excited state, S_1 , is the \tilde{A}^1A_2 state and arises from a $3s \leftarrow a_2$ excitation. This state is of great interest with regard to the photodynamics of biomolecules, as for the parent pyrrole¹² the HOMO evolves from being Rydberg in character in the FC region to σ^* character for longer N–H bond lengths, allowing for rapid photodissociation when this region of the potential energy surface is accessed; similar behavior occurs for NMP,⁹ with regard to the N–CH₃ bond length, and related molecules. This behavior is now accepted as an important mechanism for the photodissociation of biomolecules that contain heterocycles and was pioneered in theoretical work by Domcke and co-workers.^{31,32} With this Rydberg character in mind, we expect the torsional and vibrational energy levels in the S_1 state close to its potential minimum to resemble those of the ground state cation. The latter arises from a a_2^{-1} ionization, forming the $^+\tilde{X}^2A_2$ state, (the D_0^+ state) with the b_1^{-1} ionization forming the $^+\tilde{A}^2B_1$ state (the D_1^+ state). (The D_1^+ state may also be obtained from a $a_2 \leftarrow b_1$ excitation from the D_0^+ state.) With regard to the neutral electronic states that lie above the S_1 state, examination of the quantum chemical results of some of the photodynamics studies cited above indicates that their calculated ordering is dependent on the level of theory/basis set employed and/or whether vertical or adiabatic excitation energies are calculated. For these reasons, we refrain from labeling these states as $S_{n(n>1)}$ and instead label them using the following notation, in which the S_1 state is denoted as $(a_2, 3s)$:

$$\begin{aligned} \dots b_1^2 a_2^1 3p_x & \quad {}^1B_2(a_2, 3p_x), \\ \dots b_1^2 a_2^1 3p_y & \quad {}^1B_1(a_2, 3p_y), \\ \dots b_1^2 a_2^1 3p_z & \quad {}^1A_2(a_2, 3p_z), \\ \dots b_1^1 a_2^2 3s & \quad {}^1B_1(b_1, 3s), \\ \dots b_1^2 a_2^2 3p_x & \quad {}^1A_1(b_1, 3p_x), \\ \dots b_1^1 a_2^2 3p_y & \quad {}^1A_2(b_1, 3p_y), \\ \dots b_1^1 a_2^2 3p_z & \quad {}^1B_1(b_1, 3p_z). \end{aligned}$$

In the present work, the $(b_1, 3s)$ and the three $(a_2, 3p_{x,y,z})$ states are calculated to be close in energy, with the three $(b_1, 3p_{x,y,z})$ states being higher in energy; furthermore, the states within each of the $(a_2, 3p_{x,y,z})$ and $(b_1, 3p_{x,y,z})$ sets of Rydberg states are very close in energy, with the latter states being found to be overlapped by $(a_2, 3d)$ states (see Sec. IV B).

2. Vibrations

The vibrations of NMP are numbered using a scheme that has been developed by studying how the vibrations of the parent pyrrole molecule evolve as a function of the artificially varied mass of the nitrogen-bonded H atom.³³ This method examines the effects of solely changing the mass of a substituent, i.e., without any complications from steric or electronic perturbations. This is analogous to a scheme employed for monosubstituted benzenes³⁴ and extended to

the disubstituted benzenes.^{35–37} For NMP, the P_i labels employed are based on the motions of the vibrations in *N*-fluoropyrrole—further details and vibrational mode diagrams can be found in Ref. 33. We label the methyl-localized vibrations Me_i ($i = 1–9$), in descending wavenumber order, as in Ref. 33. The calculated wavenumbers for the vibrations are presented in Table II. The assignments of the S_0 vibrational wavenumbers obtained from IR and Raman studies from Refs. 23 and 24 were considered in Ref. 33. We have since become aware of another study by Beć *et al.*,²⁵ where the IR spectra of pure liquid NMP have been reported; the obtained values are quite similar to those reported in Refs. 23 and 24, and in Table II, we retain the IR/Raman values and assignments for the S_0 vibrations presented in Ref. 33.

3. Torsions and vibtor

If the methyl group is now explicitly considered, then NMP belongs to the G_{12} MSG,³⁰ and the torsional levels are described by the m quantum number, which is signed. Levels with $|m| \neq 3n$ ($n = 1, 2, \dots$) are degenerate, with the $m = 0$ level being non-degenerate. As is well known, nuclear spin and symmetry considerations mean that it is not possible to cool the $m = 1$ (strictly $|m| = 1$) torsional population into the $m = 0$ level, and hence, under the jet-cooled conditions employed herein, both levels have roughly equal populations. As a consequence, transitions can occur from either the $m = 0$ or $m = 1$ level of the S_0 zero-point vibrational level, with transitions to $m = 3n$ levels originating from the S_0 $m = 0$ level and those for $m \neq 3n$ originating from S_0 $m = 1$. We will generally refer to a level using the notation of a transition, with subscripts referring to the S_0 state and superscripts to the S_1 state, and for cationic levels, we use superscripts together with a pre-superscripted “+”; furthermore, we shall generally omit the initial level when designating a transition, as it will be clear from the excited intermediate level or the jet-cooled conditions employed. (As an example, a transition from S_0 $m = 0$ to S_1 $m = 0$ will be simply represented as m^0 .) Except where explicitly noted, vibrational transitions implicitly include transitions arising from both of the associated $m = 0$ and $m = 1$ levels, which will be almost perfectly overlapped in our spectra, as effective torsional rotational constants are very similar in the S_0 , S_1 , and D_0^+ electronic states.²⁰

Torsional levels with $|m| = 3n$ are non-degenerate, forming linear combinations for $n \neq 0$. The splitting of the $|m| = 3n$ ($n \neq 0$) levels occurs as a result of the hindered rotation and, in a G_{12} symmetry molecule, is characterized by the parameter V_6 . For example, the $m = +3$ and -3 levels form combinations that are denoted as $3(+)$ and $3(-)$, with their relative energy ordering controlled by the sign of V_6 , which is determined by the minimum energy geometry: for minimum energy geometries where the methyl group is eclipsed, with a C–H bond of the methyl group in the same plane as the pyrrolyl ring, V_6 is positive; while for a minimum staggered geometry where one of the methyl C–H bonds is perpendicular to the pyrrolyl ring, V_6 is negative. NMP has a staggered orientation in its ground electronic state but an eclipsed orientation in the S_1 state and the ground state cation.^{20,33}

B. Overview of the REMPI spectra

At the top part of Fig. 1, we show the $(1 + 1)$ REMPI spectrum of NMP over the first ~ 1110 cm^{-1} . Below this, inverted, is

TABLE II. Calculated and experimental vibrational wavenumbers (cm^{-1}) for NMP in its S_0 , S_1 , and D_0^+ states.

Sym. ^a	P_i^b	S_0			S_1			D_0^+		
		Calculated ^c	Expt.		Calculated			Expt. ^h	Calculated ^c	Expt. ⁱ
IR/Raman ^d	DF ^e		Kanamaru ^f	Woo and Kim ^g	Present work ^c					
a_1	1	3160	3130 ^j (3126)				3151		3167	
	2	3141	3103 ^j (3101)				3175		3144	
	3	1492	1504 (1509)				1534		1527	
	4	1375	1416 (1419)	1398 (1398)	1622	1510	1459	1468 (1473)	1456	
	5	1278	1286 (1288)	1281			1228		1218	
	6	1075	1088 (1091)	1092 (1083)	1162	1091	1062	1052 (1048)	1052	
	7	1045	1058 (1055)	(1058)			1104	1094	1107	
	8	956	966	933 (925)			971	968	968	
	9	652	662	669 (669)	606	635	613	635 (632)	609	629
a_2	10	863	858	857	931	931	928	907	942	937
	11	675	688	686	801	877	857	830	833	830
	12	610		611	463	520	506	468	495	498
b_1	13	814	815	815 (820)	878	891	875	824	868	861
	14	712	720	710 (718)	742	718	712	677	721	720
	15	603	601	601 (607)	376	491	482	370	490	504
	16	186	186	190 (190)	133	217	210	184	215	220
b_2	17	3152	3130 ^j (3126)				3168		3155	
	18	3132	3103 ^j (3101)				3157		3138	
	19	1505	1547		1484	1397	1372		1368	
	20	1350		(1388)	1236	1220	1187		1180	
	21	1262	1232		1388	1301	1278		1275	
	22	1073	1043		1114	1042	962	971	955	969
	23	864	868	874 (877)	730	687	659	644	646	636
	24	347	354	359 (354)			340	347	340	351
Methyl	Me ₁	3026	2942 ^j				2944		3051	
	Me ₂	2996	2942 ^j				2934		3071	
	Me ₃	2935	2819 ^j				2858		2976	
	Me ₄	1467	1464 ^j		1569	1419	1424		1463	
	Me ₅	1447	1382 ^j		1609	1449	1405		1442	
	Me ₆ ^k	1409	1382 ^j		1489	1405	1386	1390 (1394)	1408	
	Me ₇ ^l	1111	1120 ^j		1219	1138	1115	1100	1117	1113
	Me ₈	1029	1127 ^j	(1100)	935	988	1013		993	
	Me ₉ ^m	69					51		28	

^a C_{2v} symmetry labels, with the pyrrolyl ring lying in the yz -plane. The correspondence to G_{12} symmetry labels may be found in Table 1.

^bThe P_i vibrational labels are described in Ref. 33, where mode diagrams may also be found. The correspondence between the current labels and those used in Ref. 18 is provided in the supplementary material.

^cThe quantum chemical calculations undertaken for the different states were B3LYP/aug-cc-pVTZ (S_0), TD-B3LYP/aug-cc-pVTZ (S_1), and UB3LYP/aug-cc-pVTZ (D_0^+). All harmonic vibrational wavenumbers were scaled by 0.97. The calculated values for the S_0 and D_0^+ states were discussed in Ref. 33.

^dTaken from Ref. 23 and, in parentheses, Ref. 24; an occasional value comes from the force-field calculations employed in Ref. 23 (see Ref. 33).

^eFrom dispersed fluorescence experiments of the present work and, in parentheses, Ref. 18.

^fCIS/6-31G** values from Ref. 19.

^gTD-B3LYP/aug-cc-pVDZ (unscaled) values from Ref. 11 (in the supplementary material thereof).

^hFrom REMPI experiments in the present work and, in parentheses, of Ref. 11. Some values, such as those for P_{11} and P_{13} , could be affected by interactions between levels.

ⁱFrom ZEKE experiments of the present work. Some values, such as those for $^+P_9$, $^+P_{11}$, and $^+P_{13}$, could be affected by interactions between levels.

^jA unique assignment was not provided for this wavenumber.

^kThis is the methyl umbrella mode.³³

^lThis is the in-plane methyl rock.³³

^mThis is the methyl torsion.³³

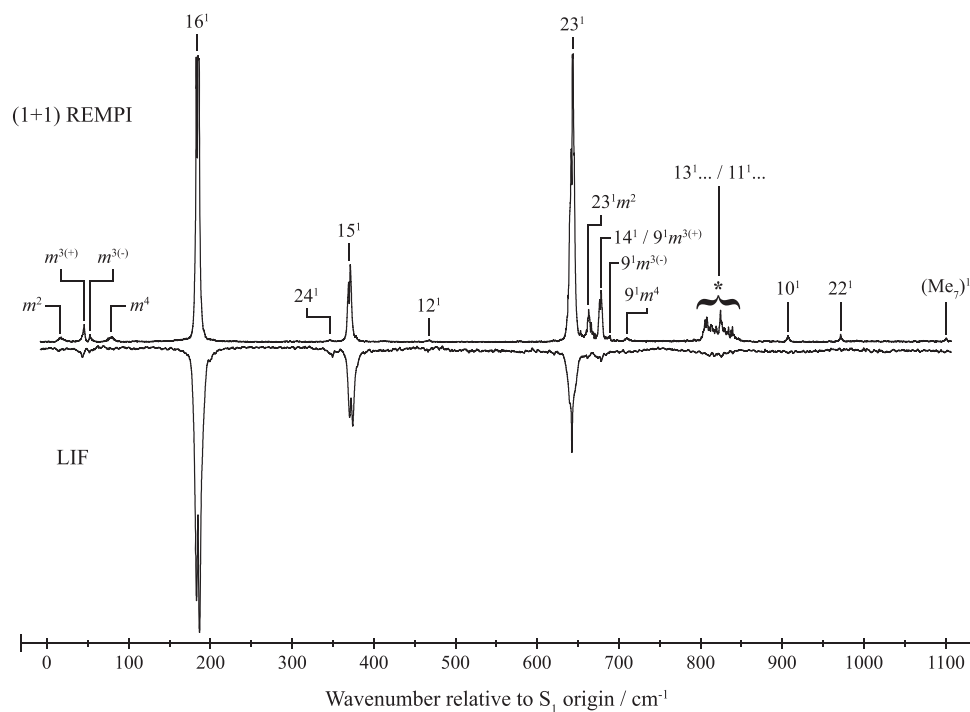


FIG. 1. Upper trace: (1 + 1) REMPI spectrum of the one-photon forbidden $S_1 \leftarrow S_0$ transition of NMP. The feature marked with an asterisk comprises multiple transitions with the associated indicated levels being the anticipated zero-order bright (ZOB) states and is shown in more detail in Fig. 12. Lower trace: reflected LIF spectrum of NMP. The LIF intensity dies off to higher wavenumbers, consistent with shorter lifetimes for the associated S_1 levels.

the corresponding LIF spectrum, and as may be seen, intensity is lost to the increasing wavenumber, particularly above $\sim 600 \text{ cm}^{-1}$, consistent with the lifetimes of the S_1 levels decreasing as the internal energy increases.^{9,11} It is the rapid absorption of a second photon in the (1 + 1) REMPI experiment that allows the higher-wavenumber region to be seen more clearly than in the LIF experiment. The (1 + 1) REMPI spectrum looks very similar to the corresponding spectra reported in earlier studies, notably that of Ref. 11, while the LIF spectrum looks similar to the limited range shown in Ref. 18. Transitions neither to the origin nor to a_1 vibrational levels are seen in either spectrum, since these are one-photon forbidden, although we do see some associated torsions.

In Fig. 2, we show the (2 + 2) REMPI spectrum of NMP in the range 0–1500 cm^{-1} , where the now-allowed origin transition²² is seen and is located at 41 193 cm^{-1} (Refs. 11 and 18). This spectrum has a narrower bandwidth than the spectra reported in earlier studies^{11,18} and the region shown in our previous work in Ref. 20, and so a more detailed structure is discernible, allowing other bands to be identified. It is clear that the only totally symmetric fundamentals are observed in the (2 + 2) REMPI spectrum, while only those for non-totally symmetric levels were observed in the (1 + 1) REMPI and LIF spectra (Fig. 1). As well as the fundamentals, some other bands are also seen (see Fig. 2), which are not straightforward to assign. The only reasonable assignment for the band at 542 cm^{-1} is $15^1 16^1$ and suggests significant anharmonicity, since by summing the

fundamentals found in the (1 + 1) REMPI spectrum, this is expected at 554 cm^{-1} . The weak band at 665 cm^{-1} is not assignable to any obvious combination band, with the vibrot transition $12^1 m^{6(-)}$ appearing to be the most likely, with it and the adjacent 24^2 band possibly gaining intensity via an interaction with 9^1 . A weak band at 1127 cm^{-1} does not have an obvious assignment, and we tentatively opt for $10^1 m^{6(-)}$, with this possibly gaining intensity from 6^1 . (Both $12^1 m^{6(-)}$ and $10^1 m^{6(-)}$ correspond to totally symmetric a_1' levels.)

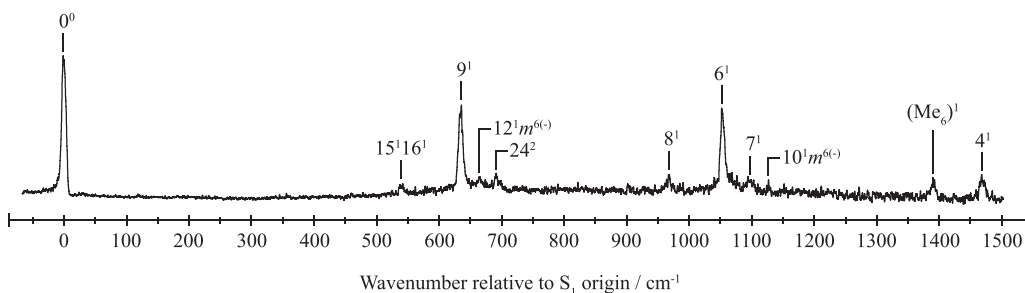
C. Vibronic coupling

As pointed out above, the $S_1 \leftarrow S_0$ ($\bar{A}^1 A_2 \leftarrow \bar{X}^1 A_1$) transition is one-photon forbidden. As such, the (1 + 1) REMPI and LIF spectra corresponding to this are dominated by vibronic transitions that are induced by vibrations of particular symmetries. In Fig. 3, a schematic energy-level diagram is shown, which indicates that there are a number of singlet states close to the $\bar{A}^1 A_2$ state: one of B_2 symmetry, two of B_1 symmetry, and, to higher energy, one of A_1 symmetry, as well as other states.

The theory of vibronic coupling is well established,^{30,38} with the transition dipole moment (TDM), M_{evt} , being given by the following:

$$M_{\text{evt}} = \int \psi'_{\text{evt}} * \mu \psi''_{\text{evt}} d\tau_{\text{evt}}, \quad (1)$$

(2+2) REMPI


FIG. 2. (2 + 2) REMPI spectrum of the two-photon allowed $S_1 \leftarrow S_0$ transition of NMP.

where ψ_{evt} are vibronic wavefunctions that also describe the torsional motion and μ is the dipole moment operator. If the wavefunctions are assumed to be completely separable, the TDM can be written as

$$M_{\text{evt}} = \int (\psi'_v \psi'_t)^* \mu (\psi''_v \psi''_t) d\tau_{\text{evt}}, \quad (2)$$

where the wavefunctions are labeled in an obvious fashion, and the integration is over all electronic, vibrational, and torsional coordinates.

If it is assumed that the electronic TDM, $M_e = \int \psi'_e \mu \psi''_e d\tau_e$, may be expanded about the equilibrium point for a vibrational or torsional coordinate, Q_i , then we can write

$$M_{\text{evt}} = \int (\psi'_v \psi'_t)^* M_e (\psi''_v \psi''_t) d\tau_{\text{vt}}, \quad (3)$$

with

$$M_e = (M_e)_{\text{eq}} + \sum_i \left(\frac{\partial M_e}{\partial Q_i} \right)_{\text{eq}} Q_i + \frac{1}{2!} \sum_{ij} \left(\frac{\partial^2 M_e}{\partial Q_i \partial Q_j} \right)_{\text{eq}} Q_i Q_j + \dots \quad (4)$$

Combining these,

$$M_{\text{evt}} = (M_e)_{\text{eq}} \int (\psi'_v \psi'_t)^* (\psi''_v \psi''_t) d\tau_{\text{vt}} + \sum_i \left(\frac{\partial M_e}{\partial Q_i} \right)_{\text{eq}} \int (\psi'_v \psi'_t)^* Q_i (\psi''_v \psi''_t) d\tau_{\text{vt}} + \frac{1}{2!} \sum_{ij} \left(\frac{\partial^2 M_e}{\partial Q_i \partial Q_j} \right)_{\text{eq}} \int (\psi'_v \psi'_t)^* Q_i Q_j (\psi''_v \psi''_t) d\tau_{\text{vt}} + \dots \quad (5)$$

For electronically allowed transitions, the first term in Eq. (5) is non-zero and is usually dominant; the observed structure depends on the overlap integral, whose square is the generalized Franck–Condon factor (FCF). Since we usually start in the (totally symmetric) zero-point vibrational level in jet-cooled experiments, then we would only expect to see transitions involving totally symmetric vibrational levels in the spectrum from this term. (In Ref. 20, we explicitly discussed the “pure” torsional levels.) The second term can also be non-zero for electronically allowed transitions, if there are nearby electronic states to steal intensity. This could affect the observed intensities of bands arising from transitions involving totally symmetric vibrational levels, but it also means that we

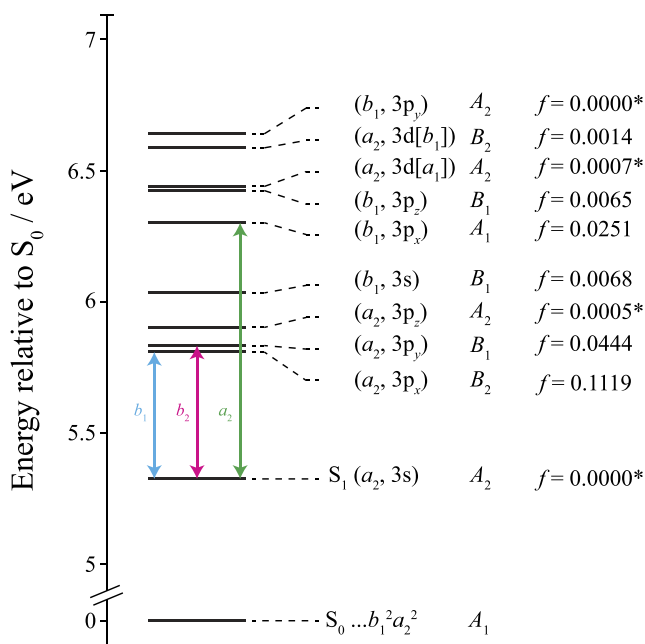


FIG. 3. Schematic, to scale, showing the calculated (TD-CAM-B3LYP/aug-cc-pVTZ) vertical excitation energies of the various singlet excited states of NMP (see also Fig. 15 and Sec. IV B). The electronic configurations are indicated in a concise format, as discussed in the text, with the electronic state symmetry indicated. Also included are the calculated oscillator strengths; those marked with an asterisk would be expected to be zero if the point symmetry were truly C_{2v} ; however, for the methyl group, the optimized geometry has C_s symmetry, and only the S_1 state is calculated to have a zero-oscillator strength here. The colored arrows indicate the main vibronic coupling routes expected, together with the symmetries of the vibrations that can induce this coupling. The b_1 symmetry vibrations (P_{13-16}) provide the dominant coupling routes, but with activity also seen involving all three a_2 symmetry vibrations (P_{10-12}) and the lower-wavenumber b_2 symmetry vibrations (P_{23} and P_{24}) (see Secs. III G 4 and IV A 3 in the text).

may see bands arising from transitions involving non-totally symmetric vibrational levels, as often seen in the spectra of substituted benzenes, for example.

For electronically forbidden transitions, such as is the case here for NMP, the first term is zero. The second term is then expected to be dominant and dictates which vibrations can induce activity and how strong the resulting transitions will be. The situation here with NMP is similar to that of benzene,^{39–41} where the transition to the first electronic state is electronically forbidden for a one-photon transition. As such, the activity observed in the excitation spectrum arises from vibrations that induce activity via the variation of the electronic dipole moment during those vibrations. An alternative way of viewing this is that the electronically forbidden transition steals intensity from an allowed transition via the inducing vibration. Thus, it is a requirement that there are allowed transitions close in energy to the electronically forbidden transition and of the correct symmetry for interaction (intensity stealing) to occur via non-totally symmetric vibrations.

Referring to Fig. 3, it can be seen that there is a 1B_2 state, ($a_2, 3p_x$), closest in energy to the S_1 state, which has the largest oscillator strength; this state can couple to the S_1 state via b_1 symmetry vibrations, as shown. Slightly higher in energy are two 1B_1 states, ($a_2, 3p_y$) and ($b_1, 3s$) that can couple with the S_1 state via b_2 symmetry vibrations; in Fig. 3, we have suggested that the activity of vibrations with b_1 symmetry mainly arises via coupling with the ($a_2, 3p_y$) state, since it is closer in energy and has the higher oscillator strength. Still higher up is an 1A_1 state, ($b_1, 3p_x$), and this can couple to the S_1 state via a_2 symmetry vibrations; this is expected to be weaker since the state is energetically further removed. Although there is also a 1A_2 state ($a_2, 3p_z$), this is also a forbidden transition, of course, and so no intensity stealing can occur from it. Except for electronic states of A_2 symmetry, the S_1 state can steal intensity from transitions to all of these states, induced by non-totally symmetric vibrations.

Similar arguments hold for torsional or vibrot levels, where the G_{12} symmetries would now need to be considered—see Table I. Hence, for example, we can expect to see a transition to the $m^{3(-)}$ level from the $m = 0$ level in the S_0 state in the one-photon absorption spectrum, via induced intensity stealing from the transition to the lowest-lying ${}^1A_1''$ (1B_2) state, since the $m = 3(-)$ level has a_2'' symmetry in the G_{12} MSG. In a similar fashion, the $m^{3(+)}$ transition can steal intensity from a transition to a ${}^1A_2''$ (1B_1) state. The arguments are the same for $m = 1$ levels, and hence, we may expect to see significant transitions to $m = 2$ and 4 levels, which is indeed the case (see Ref. 20 for further discussion). We do not see activity for m^1 nor m^5 transitions, both of which have e'' symmetry, suggesting that intensity stealing from the ${}^1A_1'$ excited level, via a_2 (a_2') symmetry vibrations, is small.²⁰

D. Expected activity in absorption

From Sec. III C and considering the first-order vibronic coupling terms for vibrations, for induced activity in the S_1 state, we require $I(\psi_{ev'}) = I(\psi_e') \times I(\psi_v')$ to correspond to an excited electronic state whose transition is one-photon allowed from the S_0 state. Referring to Fig. 3, this means that S_1 vibrations of the b_1 symmetry (P_{13} – P_{16}) can induce intensity stealing from the ($a_2, 3p_x$) 1B_2 state, and these are expected to be the strongest,

since this electronic transition has the highest calculated oscillator strength as well as being closest in energy to the S_1 state; vibrations of b_2 symmetry (P_{17} – P_{24}) can induce intensity stealing, mainly from the ($a_2, 3p_y$) 1B_1 state, and this is expected to be weaker, and vibrations of a_2 symmetry (P_{10} – P_{12}) can induce intensity stealing from the ($b_1, 3p_x$) 1A_1 state, which are expected to be the weakest. Similar comments apply to the torsional levels (see Sec. III B).

For the (2 + 2) REMPI spectrum, the situation is different, as now the $S_1 \leftarrow S_0$ transition is two-photon allowed.²² This means that the dominant vibrational activity is expected to be that determined by the FCFs, generalized to cover both torsional and vibrot transitions and hence totally symmetric levels. Indeed, Fig. 2 (and the work of Ref. 11) demonstrates that this is borne out. It is interesting that no vibronic activity is seen, which is in contrast to the allowed one-photon spectra of substituted benzenes, where both totally symmetric and vibronically induced b_2 vibrational activity is commonplace. As transitions to the required excited electronic states are still allowed in the two-photon transition,²² we conclude that such transitions must simply be too weak to see with the present sensitivity. Similar comments refer to the torsional levels, where allowed transitions would be expected to be to m^1 , as well as $m^{6(+)}$ and m^5 —the latter two are $\Delta m = 6$ transitions and so expected to be weak; neither are observed.

E. Expected activity in emission

Similar arguments apply to emission as for one-photon absorption, except now we are commencing at vibrational levels in the S_1 state that are non-totally symmetric. With the excitation laser, we can select levels of different symmetry in the S_1 state and observe the emission from these; in the free-jet expansion, little vibrational or torsional relaxation in the S_1 state will occur. We now expect the dominant emission activity to be that corresponding to the initially excited vibration but in combination with the inducing vibrations of b_1, b_2 , and (weaker) a_2 symmetry, with the first of these dominating. As will be seen, again these expectations are largely borne out and are consistent with the activity seen in the corresponding spectra of benzene.^{39–41}

We comment that Biswas *et al.*¹⁸ reported DF spectra of NMP when exciting via a number of S_1 torsional levels and also $16^1, 15^1$, and 24^1 . (We have transcribed their numbering into that employed herein, with the correspondence included in Table SI of the supplementary material.) The presentation of the DF spectra in that work is somewhat difficult to follow, with the same numbered band corresponding to different terminating levels. We have discussed the torsional levels in Ref. 20, and we will see that for many of the vibrational assignments, we agree with those in Ref. 18 for the DF spectra obtained via the three lowest S_1 vibrational levels. In the present work, we shall see evidence for more widespread vibronic coupling, examine more levels by both DF and a selected number with 2D-LIF, and for the first time, report ZEKE spectra of almost all levels having $<1110 \text{ cm}^{-1}$ internal energy in the S_1 state, observed in the (1 + 1) REMPI spectrum. In so doing, we obtain reliable gas-phase values for a significant number of vibrational wavenumbers in the S_0 and S_1 states and will compare to previous assignments; for the D_0^+ state, we report vibrational wavenumbers for the first time.

We highlight that, although not emphasized in Ref. 20, we found the 2D-LIF spectrum recorded for the torsional levels of NMP to be dominated by 15_1m_x and 16_1m_x bands, at the positions where the m^x transition was excited; this is consistent with activity seen herein for the vibrations.

F. ZEKE spectra

Since it is known that the S_1 state is largely 3s Rydberg-like in the FC region, then we expect the ZEKE spectra to be dominated by $\Delta m = 0$, $\Delta v = 0$, or $\Delta(v, m) = 0$ bands, as appropriate, since the S_1 and D_0^+ geometries are expected to be very similar; this is in line with the results of quantum chemical calculations.²⁰ This was indeed the case for the ZEKE spectra via the torsional levels,²⁰ and as will be seen, this is also the case for many of the vibrations and vibrot levels in the present work. Additionally, it would also be expected that the wavenumbers for corresponding vibrations would be very similar for the S_1 and the D_0^+ states. Indeed, looking at the calculated wavenumbers in Table II, the values are very similar across all vibrations for these two electronic states. In contrast, there are some exceptions to this expectation for some of the experimental values, most notably for vibrations of b_1 symmetry but also those of a_2 symmetry, and this will be discussed in Secs. III G 4 and IV A 3.

G. Spectra and assignments

1. DF and 2D-LIF spectra via 16^1

In Fig. 4, we show the DF and 2D-LIF spectra obtained following excitation to the S_1 b_1 symmetry vibration, 16^1 . In overall appearance, the DF spectrum is similar to that reported by Biswas *et al.*,¹⁸ except that the present spectrum is of higher resolution. We can see that the two most intense bands are those corresponding to 16_2 and 15_116_1 , confirming that P_{15} and P_{16} are the vibrations that induce the majority of the vibronic interaction, via the $(a_2, 3p_x) ^1B_2$ state; we also see combination bands involving the other b_1 symmetry vibrations 14_116_1 and 13_116_1 , as well as the 15_2 band. In addition, we see activity induced by a b_2 vibration, 16_23_1 , and two induced by a_2 vibrations, 11_116_1 and 10_116_1 . (If 12_116_1 is present, it would be overlapped by 15_116_1 .) There are various other bands, presumably associated with small structural changes, of the same overall vibrational symmetry as the induced bands, but there are multiple possibilities for some of the bands to higher wavenumbers, and so we refrain from giving all of those an explicit assignment. The given assignments allow the wavenumbers for a number of S_0 vibrations to be determined, as well as 16^1 in the S_1 state; these are collected together in Table II and concur with those obtained from other spectra discussed in the present work.

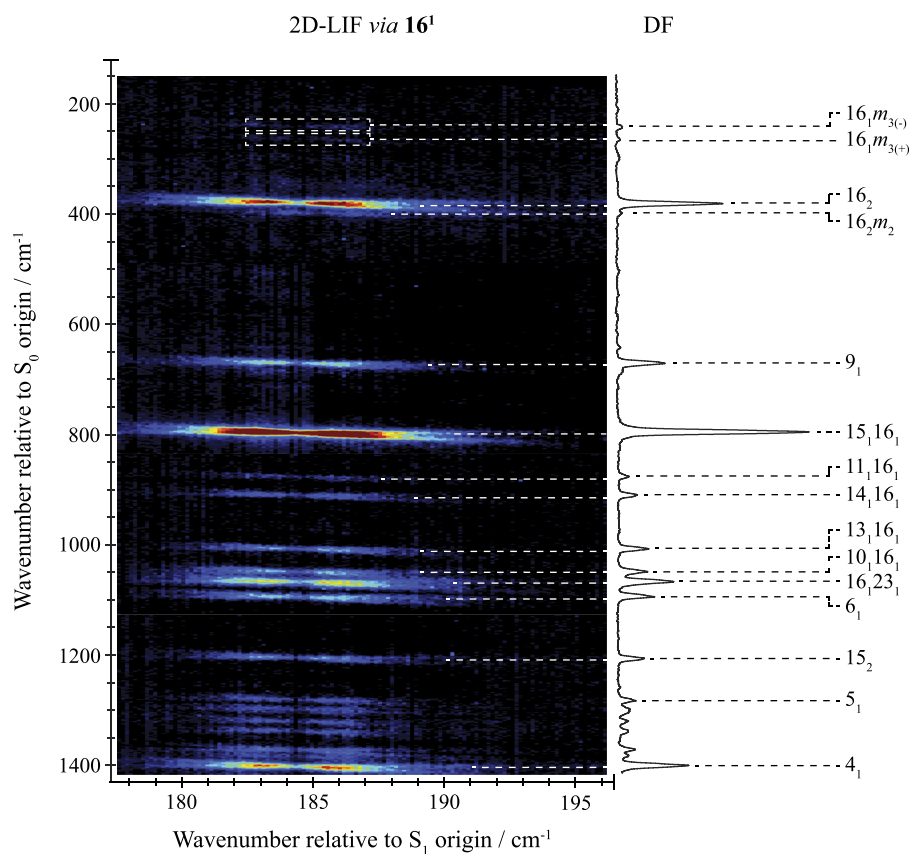


FIG. 4. DF and 2D-LIF spectrum via 16^1 . Assignments are given for many of the bands, which are consistent with vibronic coupling, and are discussed further in the text.

We highlight that we see both the $16_1 m_{3(-)}$ and $16_1 m_{3(+)}$ bands, whose activity could be induced by the corresponding torsions, involving the $(a_2, 3p_x) {}^1B_2 ({}^1A_1'')$ and $(a_2, 3p_y) {}^1B_1 ({}^1A_2'')$ electronic states, respectively. This pair of bands was also seen when exciting the $m^{3(+)}$ and $m^{3(-)}$ levels.²⁰

The simple appearance of the isolated 16^1 band in the REMPI and LIF spectra (Fig. 1) indicates that it is unlikely that 16^1 is interacting significantly with any other level in the S_1 state, and the 2D-LIF spectrum supports this, in that the main activity is localized, with a distinctive band shape, and no indications of any overlapping features are apparent.

We shall discuss the ZEKE spectrum from 16^1 in Sec. III G 4.

2. DF and 2D-LIF spectra via 15^1

The DF and 2D-LIF spectra recorded via the S_1 15^1 level, also a b_1 symmetry vibration, are shown in Fig. 5. The DF spectrum is

similar to that reported by Biswas *et al.*,¹⁸ and we agree with their assignments, but again the present spectrum is of higher resolution. In a similar way to the DF spectrum from S_1 16^1 , we see strong activity induced by b_1 symmetry vibrations, with the 15_2 band being the most intense, but we also see combination bands associated with the other b_1 symmetry vibrations, $15_1 16_1$, $14_1 15_1$, and $13_1 15_1$, together with the 16_2 band. Additionally, we see the transition induced by a b_2 symmetry vibration, $15_1 23_1$, as well as $16_1 23_1$; possible bands induced by a_2 vibrations, $11_1 15_1$ and $10_1 15_1$, are very weak and are not marked; in addition, if the $12_1 15_1$ band is present, it would lie under 15_2 . There are various other bands, but we refrain from giving explicit assignments when there is more than one reasonable possibility. We do not see the $15_1 m_{3(-)}$ and $15_1 m_{3(+)}$ vibronic bands, although these were seen when exciting via $m^{3(+)}$ and $m^{3(-)}$.²⁰ A weak band that is at the correct wavenumber to correspond to the a_1' symmetry $m_{6(+)}$ is tentatively assigned as such. Assignment of the

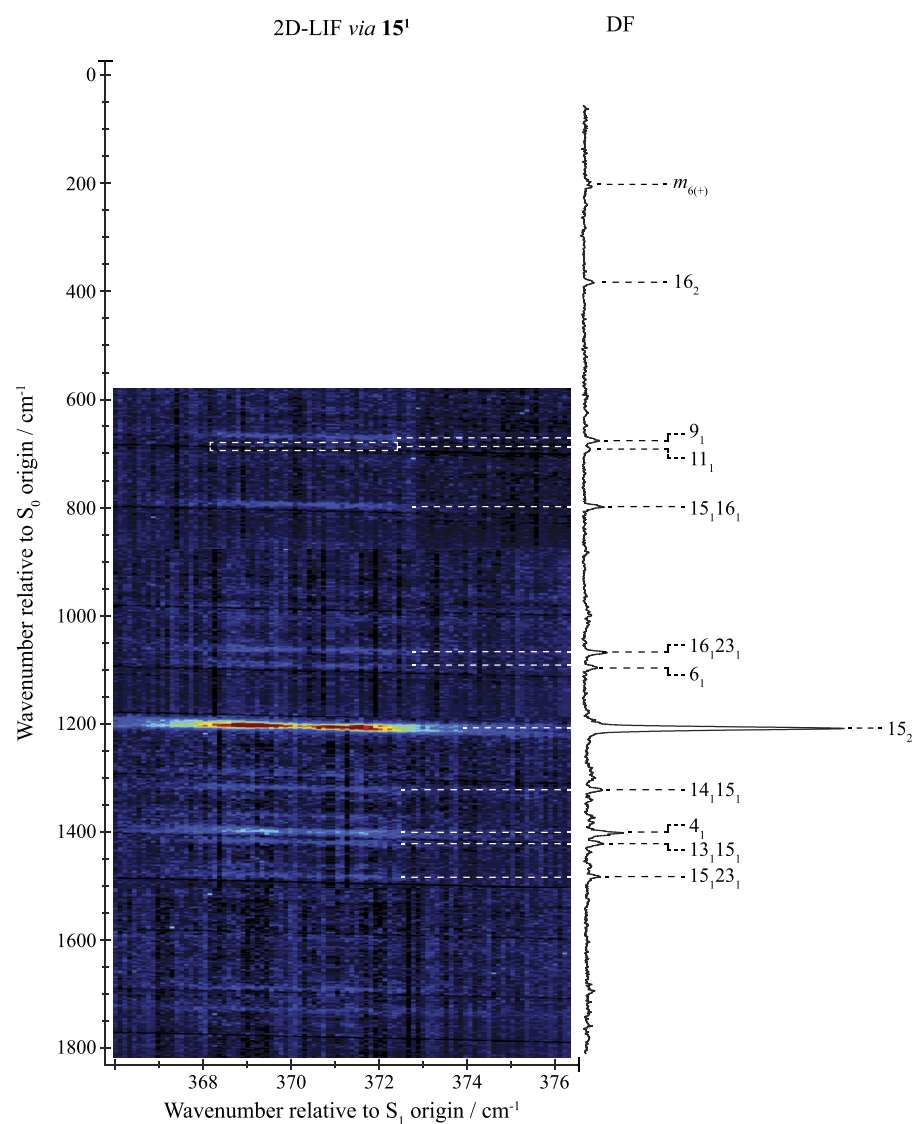


FIG. 5. DF and 2D-LIF spectrum via 15^1 . Assignments are given for many of the bands, which are consistent with vibronic coupling, and are discussed further in the text.

spectra allows a number of vibrational wavenumbers for the S_0 state to be determined, as well as 15^1 in the S_1 state; these are collected together in Table II.

The REMPI and LIF spectra (Fig. 1) indicate that it is unlikely that, as with 16^1 , the 15^1 level is interacting with any other level in the S_1 state, and the 2D-LIF spectrum again supports this, in that the main activity is localized, with a distinctive band shape, and no indications of any overlapping features are apparent.

We shall discuss the ZEKE spectrum from 15^1 in Sec. III G 4.

3. DF spectrum via 14^1

In Fig. 6, we show the DF spectrum recorded via 14^1 . This is dominated by the $14_1 15_1$ band, with $14_1 16_1$, 14_2 , and $13_1 14_1$ also being seen—all induced by b_1 symmetry vibrations; bands induced by a_2 symmetry vibrations are not observed here, although $12_1 14_1$ would be overlapped by the $14_1 15_1$ band. Furthermore, bands induced by a_2 and b_2 symmetry vibrations are also present. These assignments allow a number of vibrational wavenumbers for the S_0 state to be determined, as well as 14^1 in the S_1 state; these are collected together in Table II. This spectrum has not been reported previously.

We shall discuss the ZEKE spectrum from 14^1 in Secs. III G 4 and III G 6.

4. ZEKE and PIE spectra via 16^1 , 15^1 , and 14^1

In Fig. 7, we show the ZEKE spectra recorded via each of the S_1 vibrational levels 16^1 , 15^1 , and 14^1 , all of which are of b_1 symmetry. In addition, for each intermediate, we superimpose the PIE curve for production of NMP^+ , covering the main activity in each ZEKE spectrum.

The ZEKE spectrum recorded via 14^1 is largely as expected, with the strong $\Delta v = 0$, $^+14^1$, band dominating. There is a weak, symmetry forbidden $^+m^{0,1}$ band, but it is not possible to see other transitions to pure torsional levels. The feature with multiple contributions across the range 635–700 cm^{-1} (marked with an obelus) will be discussed further in Sec. III G 6.

Although there is no clear onset, we see that the PIE curve via 14^1 shows activity close to the AIE, consistent with the weak $^+m^{0,1}$ ZEKE band, and this continues up to a sharp rise at the position of the $\Delta v = 0$ band, $^+14^1$, as expected. Unexpected, however, is the sharp drop-off in the PIE intensity at $\sim 800 \text{ cm}^{-1}$. Indeed, as can be seen in Fig. 7, the PIEs recorded via the 14^1 , 15^1 , and

16^1 levels all show such a drop-off, albeit at different wavenumbers. Not shown in Fig. 7 is that the PIE intensity picks up again in all cases to higher wavenumbers and appears to be associated with the absorption of more than one photon from the ionization laser. We are currently investigating this behavior, and the structure that appears in some regions of the PIE curves, and will report our findings in due course;⁴² for the purposes of the present work, only the regions of the PIE curves before the drop-offs are pertinent.

In some ways, the ZEKE spectrum recorded via 16^1 is largely as expected, with the $\Delta v = 0$ band being by far the most intense—in line with expectations based upon the Rydberg character of the S_1 level and activity seen in other ZEKE spectra. Moreover, the wavenumber for $^+16^1$ (220 cm^{-1}) is in very good agreement with the calculated value. It is notable that the experimental wavenumber value for the 16^1 level in the S_1 state (184 cm^{-1}) is significantly lower than both the cation value and the calculated value. This will be discussed further in Sec. IV A 3. Also seen in the ZEKE spectrum via 16^1 are bands associated with $^+m^{0,1}$, $^+m^2$ (as a shoulder on the $^+m^{0,1}$ band), and $^+m^4$; a weak band that seems to contain contributions from both $^+m^{3(+)}$ and $^+m^{3(-)}$ is also seen. The torsional potentials in the S_1 and D_0^+ states are very similar, in particular, the sign of the V_6 parameter and its almost identical magnitude.²⁰ As such, the torsional levels in both states are at very similar wavenumbers. With regard to the PIE curve, we see a clear onset at the AIE, followed by a plateau with some structure, and then a sharp rise at the position of the $\Delta v = 0$ band, $^+16^1$, as expected, followed by the aforementioned drop-off in intensity, this time at $\sim 320 \text{ cm}^{-1}$.

Looking now at the ZEKE spectrum recorded via 15^1 , we see unexpected behavior: the $^+15^1$ ZEKE band that is observed at 504 cm^{-1} (Table II) is not the strongest band; this is despite the expected behavior seen for the DF and 2D-LIF spectra recorded from this level (see Sec. III G 2). We actually find the strongest band to be $^+16^1$. As with the 16^1 ZEKE spectrum, we see a reasonably intense origin ($^+m^0$ and $^+m^1$) and bands associated with $^+m^2$ and $^+m^{3(+)} / ^+m^{3(-)}$. In the 345–475 cm^{-1} range, marked with an asterisk in Fig. 7(b), there is a complicated set of bands. The only possible NMP contributions to this region would be $^+24^1 m^x$ vibrotor levels, and although there are possibilities of interactions in the S_1 state with the $15^1 m^x$ vibrotor levels, such as an indirect $15^1 m^1 \dots 24^1 m^1$ interaction, explaining the presence of the $^+24^1 m^1$ band, there are no obvious signs of interactions in the 2D-LIF

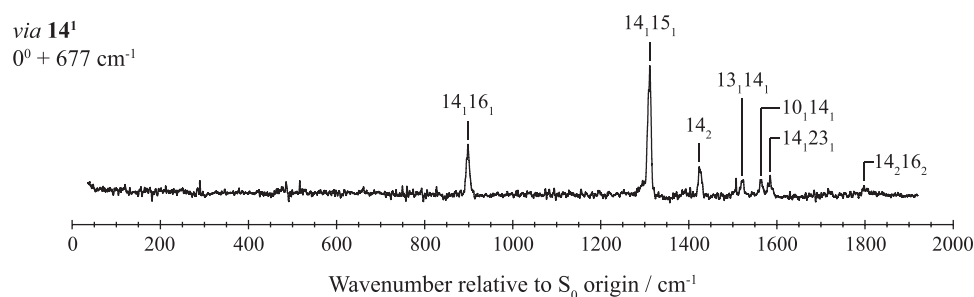


FIG. 6. DF spectra for 14^1 . Assignments are given for many of the bands, which are consistent with vibronic coupling, and are discussed further in the text.

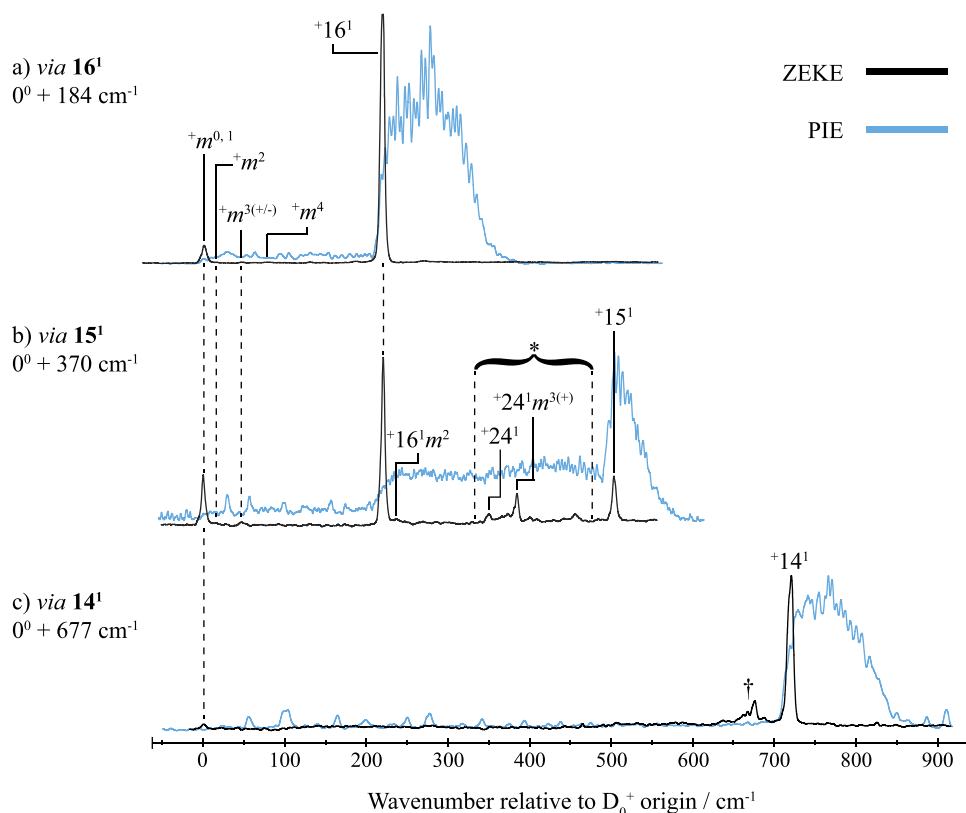


FIG. 7. ZEKE and PIE spectra via (a) 16^1 ; (b) 15^1 ; and (c) 14^1 . The sharp drop-offs in the intensities of the PIE curves to high wavenumbers are genuine and will be discussed in future work,⁴² as will the structure in the low-wavenumber region of the PIE curves. The ZEKE spectrum for 14^1 is that expected for ionization from a Rydberg state, while the other two spectra have unexpected aspects that are discussed further in the text. The relative weakness of the $^+15^1 \Delta\nu = 0$ band in (b) is striking and is commented on further in the text. The region marked with an asterisk in (b) is likely due contributions from $^+24^1 m^x$ together with a serendipitous overlap with an NMP-Ar resonance at this excitation energy.⁴² The 14^1 band is overlapped by $9^1 m^{3(+)}$, which is responsible for the feature marked with an obelus (\dagger) (see Fig. 10 and text).

spectrum (see Sec. III G 2). The $^+24^1 m^{3(+)}$ level is totally symmetric, and its presence is consistent with the appearance of the origin band. In fact, ongoing experiments⁴² indicate that, as well as the $^+24^1 m^1$ and $^+24^1 m^{3(+)}$ bands, the 345–475 cm^{-1} region has contributions from NMP-Ar, owing to an overlapping resonance at this excitation energy.

Looking now at the PIE curve recorded via 15^1 , we see more-expected behavior. As with the 14^1 and 16^1 PIE curves, we see an onset at the AIE, with structure, followed by a plateau. Although we then see a clear onset corresponding to a non- $\Delta\nu = 0$ band, $^+16$, consistent with the ZEKE spectrum, this is followed by the expected sharp rise corresponding to the $\Delta\nu = 0$ transition, $^+15^1$, with this latter rise being larger than that of the $^+16^1$ step. Thus, from the point of view of the PIE curve, this photoionization behavior is as expected, with the strongest rise being the $\Delta\nu = 0$ band, which appears in the expected position, and consistent with a value for $^+15^1$ of 504 cm^{-1} and close to the calculated value (Table II). The less-intense $^+15^1$ ZEKE signal is thus highly surprising; indeed, we have recorded this spectrum under a range of conditions, and the band is actually absent on some occasions, suggesting a sensitive

dependence on experimental conditions. In addition, the appearance of the $^+16^1$ band when exciting via $^+15^1$ is also somewhat unexpected as, even though it is symmetry allowed, we are expecting largely diagonal FCFs.

The lack of $^+16^1$ and $^+15^1$ ZEKE bands when exciting via 14^1 is in line with expectations. However, given the observed strong activity of $^+16^1$ when exciting via 15^1 , then we might have expected some activity from $^+15^1$ when exciting via 16^1 , given the aforementioned $^+16^1$ activity via 15^1 . However, as can be seen in Fig. 7, there is a complete drop-off of ionization cross section for each of the PIE curves to higher wavenumbers; that is, no ions, including fragment ions, are seen that are attributable to ionization of NMP in these regions. This observation is a possible explanation for the absence of the $^+15^1$ band when exciting via 16^1 , as the $^+15^1$ band would appear in this drop-off region. In addition, this may have some bearing on the relative weakness of the $\Delta\nu = 0^+15^1$ band when exciting via 15^1 , with other possibilities involving a Rydberg state “window resonance” (i.e., an interaction with a Rydberg state with a low ionization cross section and so reduction of signal) or highly efficient autoionization at the $^+15^1$ position (and so depleting the

number of ZEKE electrons produced). It is clear that the diminished $^{+}15^1$ ZEKE signal is not directly related to the S_1 state as we see the expected emission activity (Sec. III G 2) and a significant step in the PIE curve at the expected wavenumber of $^{+}15^1$. Further experiments on the photoionization behavior via these features is ongoing.⁴²

We highlight the close agreement of the calculated S_1 and D_0^+ wavenumbers for these three b_1 symmetry vibrations (Table II). Furthermore, the experimental D_0^+ wavenumbers are very close to the calculated ones. With these points taken together with the deviation of the experimental values of the S_1 state from the calculated ones, they suggest a change in shape of the actual S_1 potential along b_1 symmetry coordinates away from that expected from its $3s$ Rydberg character close to the potential minimum. (The experimental S_1 vibrational wavenumber for 15^1 is 370 cm^{-1} , a shift of $\sim 23\%$ from the calculated value; that for 16^1 is slightly lower at $\sim 12\%$; and for 14^1 , the shift is smaller still at $\sim 5\%$, while for the final b_1 symmetry vibration, 13^1 , the shift is $\sim 6\%$ —see Table II.) In Sec. IV A 3, we shall discuss these shifts in wavenumbers in more detail, but this does not seem to be related to evolution of the S_1 HOMO to σ^* character along the N-CH₃ coordinate, which would only be expected to change the potential along a_1 symmetry coordinates.

In passing, we comment that although 16^2 is expected to have a value close to the 370 cm^{-1} value in S_1 , it is of the wrong symmetry to be active via a one-photon transition, and, furthermore, $^{+}16^2$ in the cation would be expected at 440 cm^{-1} and no such band is seen.

5. DF and ZEKE spectra via 24^1 and fluorescence spectra via 23^1

The DF spectrum recorded via 24^1 is shown in Fig. 8 and shows prominent 16_124_1 and 15_124_1 bands; in addition, we see the weaker 14_124_1 , 13_124_1 , 10_124_1 , and 23_124_1 bands. This confirms that the same b_1 vibrations are inducing the main activity in emission, even when the intermediate has a different symmetry, and that the other vibronic mechanisms are also operating similarly. Interestingly, the 14_124_1 band appears to be $\sim 10\text{ cm}^{-1}$ higher than expected, but no other sensible assignment is apparent: although 24_3 fits better in terms of wavenumber, we do not expect to see this band. (It is a pity that the 14_124_1 band was not observed when exciting 14^1 , see Fig. 6, which would have confirmed this shifted band position.) Other bands to higher wavenumbers do not have unambiguous assignments. Assignment of the spectrum allows a number of vibrational wavenumbers for the S_0 state to be determined, as well as S_1 24^1 itself; these are collected together in Table II. The assignment of the DF spectrum largely agrees with that of Biswas *et al.*¹⁸

In addition, in Fig. 8, we also include the ZEKE spectrum recorded via 24^1 . The assignment of this spectrum is clear, since it is dominated by the $\Delta v = 0$ band and yields a wavenumber for the $^{+}24^1$ vibration of 351 cm^{-1} .

The DF and 2D-LIF spectra recorded via 23^1 are presented in Fig. 9. The spectrum is largely as expected, with prominent 15_123_1 and 16_123_1 bands and weaker 14_123_1 , 13_123_1 , and 23_2 bands; both the 16_1 and 15_1 bands are also seen. In addition, there are various other bands to which we are unable to give unique assignments. The given assignment of the spectra allows a number of vibrational

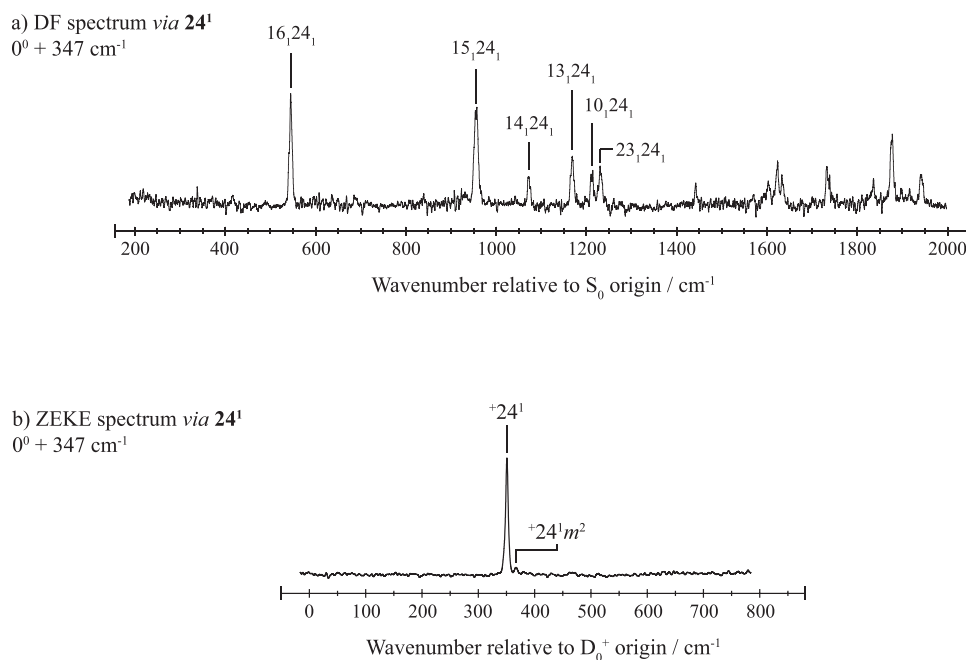


FIG. 8. (a) DF spectrum via 24^1 . Assignments are given for many of the bands, which are consistent with vibronic coupling, and are discussed further in the text. (b) ZEKE spectrum via 24^1 .

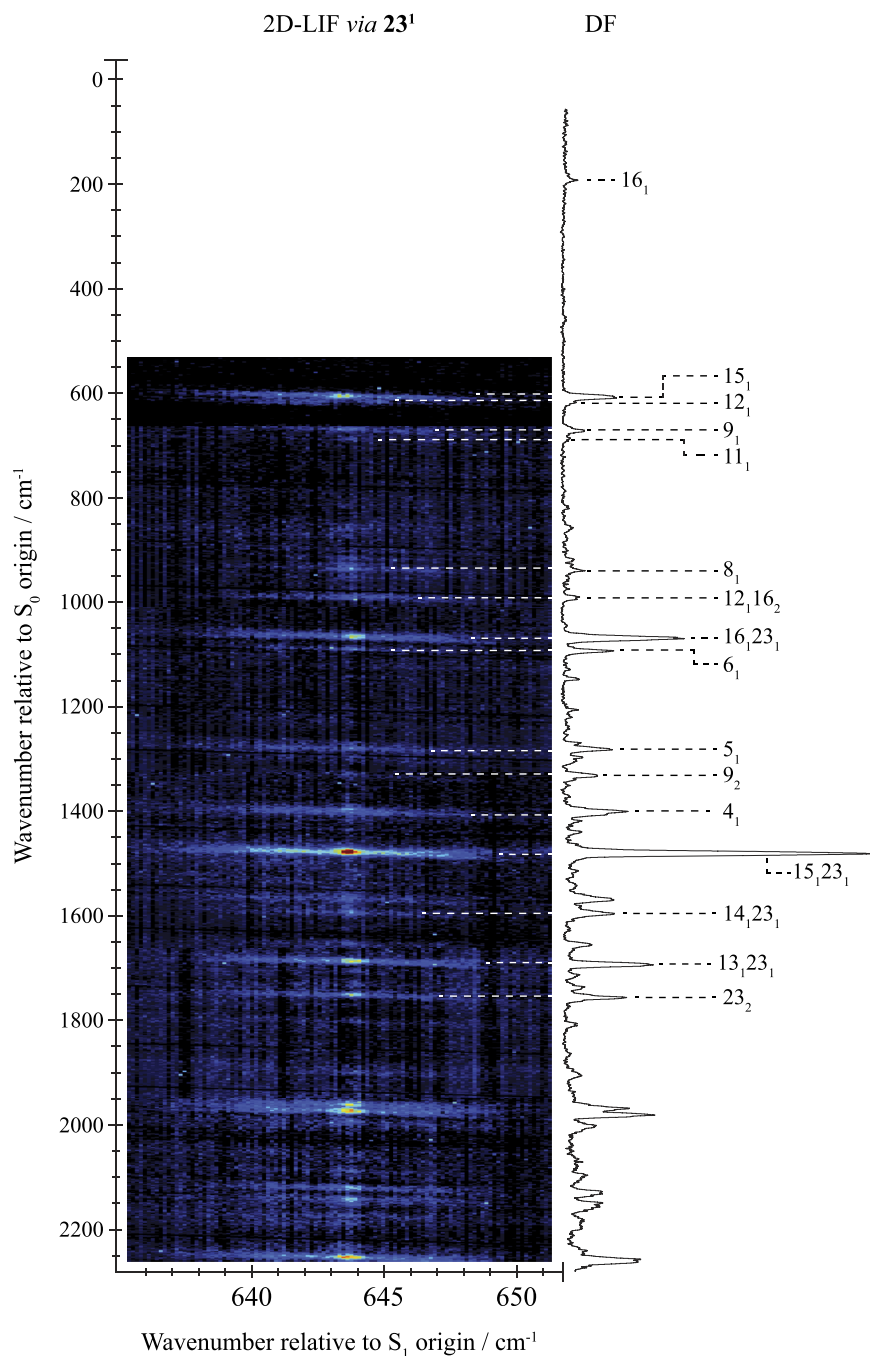


FIG. 9. DF and 2D-LIF spectrum via 23^1 . Assignments are given for many of the bands, which are consistent with vibronic coupling, and are discussed further in the text.

wavenumbers for the S_0 state to be determined, as well as 23^1 itself; these are collected together in Table II. These spectra have not been reported previously.

Although there are a number of bands in close proximity in the $(1 + 1)$ REMPI and LIF spectra, over the region scanned, the 2D-LIF spectrum does not give any clear indication that interactions are occurring, with each band showing the same distinctive profile. However, the ZEKE spectra recorded over this region, and which are

discussed in Sec. III G 6, do show evidence of some interactions in this region of the spectrum, and it is possible that a 2D-LIF spectrum over the whole $630\text{--}720\text{ cm}^{-1}$ region would show further evidence for this, but would be very time consuming to obtain.

6. ZEKE spectra via bands in the $630\text{--}720\text{ cm}^{-1}$ region

There is a very intense band in the $630\text{--}720\text{ cm}^{-1}$ region, with a number of bands to higher wavenumbers. ZEKE spectra have been

recorded through all of the main bands and the observed activity, and these are presented in Fig. 10. The expectation of close-to-diagonal FCFs allows the assignment of the S_1 levels. We have already presented (Fig. 7) the ZEKE spectrum via 14^1 (at 677 cm^{-1}) in Sec. III G 4, together with the PIE curve. We have included the ZEKE spectrum again in Fig. 10 to allow facile comparison with the other spectra in this region and allow discussion of the assignments of the weaker features, which have not already been discussed.

The most intense band at 644 cm^{-1} has been assigned to 23^1 on the basis of the DF and 2D-LIF spectrum, discussed in Sec. III G 5, and again, the ZEKE spectrum confirms that this is the major contributor, yielding the wavenumber for the D_0^+ vibration of 636 cm^{-1} . We highlight how close the corresponding values are for both the S_1 and D_0^+ electronic states, in line with the $3s$ Rydberg character of the former.

The assignment of the other ZEKE spectra are now discussed—no DF spectrum could be recorded for these bands, except for 14^1 (Fig. 6), owing to the diminishing lifetimes of the levels as the internal energy in the S_1 state increases. We first

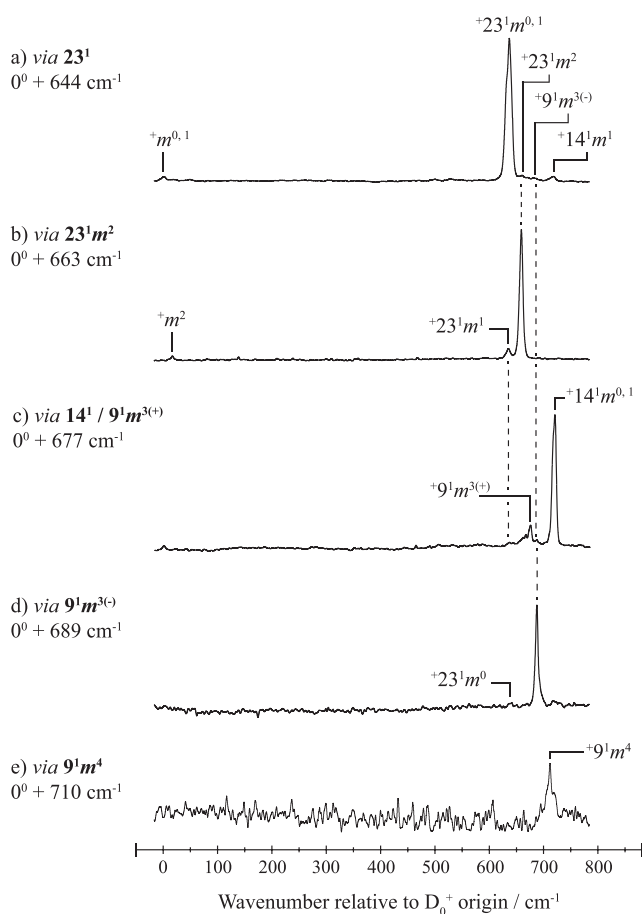


FIG. 10. ZEKE spectra via levels in the $635\text{--}715\text{ cm}^{-1}$ region of the $(1 + 1)$ REMPI spectrum.

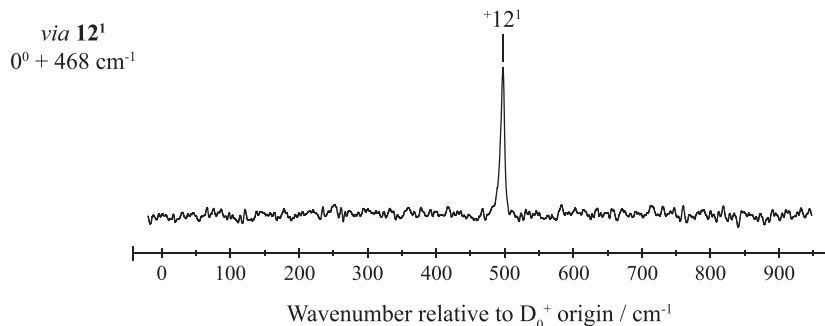
mention that the band at 663 cm^{-1} in the $(1 + 1)$ REMPI and LIF spectra is straightforwardly assignable to 23^1m^2 since, first, the ZEKE spectrum demonstrates a strong $\Delta(v, m) = 0$ band, $+23^1m^2$, at 658 cm^{-1} , as expected, and second also shows a clear $+m^2$ band, with $+23^1m^1$ also clearly observable.

The other weaker features in the $(1 + 1)$ REMPI spectrum to higher wavenumbers are not in the correct place to be other 23^1m^x vibrotor levels, and so another assignment was sought. Aided by the observed torsional structure related to the forbidden origin band in the $(1 + 1)$ REMPI spectrum²⁰ and by the location of the 9^1 transition at 635 cm^{-1} that is assigned in the $(2 + 2)$ spectrum (Fig. 2 and Ref. 11), we expect to see 9^1m^x vibrotor transitions in this region of the spectrum. Indeed, two of the higher wavenumber bands are at the correct wavenumber to be $9^1m^{3(-)}$ and 9^1m^4 . The 9^1m^2 band can be seen weakly between 23^1 and 23^1m^2 (not labeled in Fig. 1), while $9^1m^{3(+)}$ will be overlapped by 14^1 [see Figs. 1 and 10(c)]. No ZEKE spectrum was recorded via the very weak 9^1m^2 band, with the ZEKE spectra via 9^1m^4 and $9^1m^{3(-)}$ being dominated by a single band—see Fig. 10. The observation of the weaker feature in the ZEKE spectrum recorded via 14^1 , whose wavenumber is consistent with a contribution from $+9^1m^{3(+)}$, confirms that these two bands overlap at $\sim 677\text{ cm}^{-1}$. There is some slight variation from the vibrotor band positions expected, when employing the value for 9^1 obtained from the $(2 + 2)$ REMPI spectrum. This could be partly related to the width of the $(2 + 2)$ REMPI bands but also could be due to interactions, such as $23^1m^0 \dots 9^1m^{3(+)}$, $14^1m^0 \dots 9^1m^{3(-)}$, and $23^1m^1 \dots 9^1m^2 \dots 14^1m^1$, with the latter allowing an indirect coupling between 23^1m^1 and 14^1m^1 . As well as slightly shifted REMPI band positions, the activity in the ZEKE spectra shows some evidence of such interactions. For example, there is a weak band seen in the ZEKE spectrum via 23^1 that can be assigned as $+14^1m^1$; there is also weak cross-activity between the 14^1m^0 and $9^1m^{3(-)}$ spectra. We comment that seeing such interactions in the ZEKE spectra here is made difficult for some levels, since the torsional and in-plane (a_1 and b_2 symmetry) vibrations are almost identical in the S_1 and D_0^+ states so that any interaction would be expected to occur in both states; hence, vertical transitions will be between the same eigenstates with the same composition. For the out-of-plane vibrations (a_2 and b_1 symmetry), however, there are significant shifts between the two levels, which is consistent with an assignment of $+14^1$ for the weak, higher-wavenumber feature seen in the ZEKE spectrum via 23^1 , arising from the indirect $23^1m^1 \dots 9^1m^2 \dots 14^1m^1$ interaction.

7. ZEKE spectrum via 12^1

The ZEKE spectrum via the a_2 symmetry 12^1 level is shown in Fig. 11 and demonstrates an essentially perfectly diagonal FCF, with a single band appearing at 498 cm^{-1} , which is in excellent agreement with the calculated wavenumber for $+12^1$, supporting the assignment. Owing to the weakness of the 12^1 band in fluorescence, no DF spectrum could be recorded for this level.

There is some possible ambiguity between the assignment of bands associated with the P_{12} and P_{15} vibrations, as these are calculated to have very similar wavenumbers in all three electronic states under consideration. However, the different symmetries, the expected vibronic coupling, and the DF and 2D-LIF spectra for 15^1

FIG. 11. ZEKE spectrum via 12^1 .

are highly supportive of the assignment of 15^1 to the strong 370 cm^{-1} band, supporting a shifted vibrational wavenumber as the result of the vibronic interaction. This makes the assignment of the significantly weaker 468 cm^{-1} band to 12^1 secure and hence also establishes the corresponding vibrational wavenumbers in the S_1 and D_0^+ states. The 12^1 assignment is also in line with the observation of transitions involving the other two a_2 symmetry vibrations, 10^1 and 11^1 , discussed in Secs. III G 8 and III G 9.

8. ZEKE spectra via the 800 cm^{-1} feature

In the $800\text{--}850\text{ cm}^{-1}$ region of the $(1+1)$ REMPI spectrum, a complicated feature is seen, which is shown in Fig. 1 and in an expanded form at the top of Fig. 12. Although this feature has been referred to previously,¹¹ the clear complexity of the feature has not; it is evident that there are a number of contributions. To gain insight into these, we have recorded eleven ZEKE spectra at different positions across the band, as indicated in Fig. 12; these have been normalized to the most intense band in each case. Below the $\Delta\nu = 0$ bands at $\sim 750\text{ cm}^{-1}$, we have amplified the intensity by a factor of 4 to highlight the weak structure, which turns out to be crucial to the assignment, and we have also provided expanded views of the $\Delta\nu = 0$ regions on the right-hand side of Fig. 12. Although an attempt was made at recording a DF spectrum via the most intense part of this band, this yielded a noisy spectrum, with very few features discernible; this is in line with the very stark reduction in intensity in the LIF spectrum compared to the REMPI spectrum—see Fig. 1. Furthermore, the distinct structure seen in the REMPI spectrum over this region was not resolved in the LIF spectrum, meaning that any comparison between DF spectra, or even a 2D-LIF spectrum, over this region would have proved challenging.

The assignment of the ZEKE spectra in Fig. 12 makes use of the fact that we generally expect largely diagonal FCFs. It is clear that there are a number of contributions across this region, and the ZEKE spectra suggest that various interactions are occurring between various zero-order states (ZOSs). The contributions will consist of one or more zero-order bright (ZOB) states, interacting with various zero-order dark (ZOD) states, to produce various eigenstates, which may comprise vibrational and torsional contributions; we do not consider rotations. Inspection of the values in Table II and comparing with the ZEKE spectra, taking into consideration the excitation wavenumber range, suggests that there are two likely fundamental ZOB states, 11^1 and 13^1 , each of which has $m = 0$ and $m = 1$

components; both of these were suggested as contributing to this region of the spectrum in Ref. 11. In Table III, we summarize the vibrational and vibtor levels that are of the same symmetry as these ZOB states and that may be contributing to this energy region. These values can only be used as a guide initially, since levels of the same symmetry may interact, leading to slightly shifted eigenstates. As well as the fundamentals, Table III shows that there are also vibrational combinations, which could be either ZOB states or ZOD states, $9^1 16^1$, $12^1 24^1$, and $16^1 23^1$, the first two of which can interact with 13^1 , while the latter one can interact with 11^1 . Activity involving both 13^1 and 11^1 would be in line with other transitions seen in the REMPI spectrum (see Fig. 1), with the b_1 symmetry 13^1 state expected to be the brighter, owing to the closer proximity and higher oscillator strength of the 1B_2 state from which it is stealing its intensity (see Fig. 3).

The complicated nature of the $800\text{--}850\text{ cm}^{-1}$ excitation feature suggests that there are a number of vibrational/vibtor levels interacting. Taking account of the wavenumbers and symmetries of vibrations in the S_1 state, the expected torsional spacings, and the ZEKE activity, the following vibrational interactions (represented by "...") might be expected, with corresponding interactions occurring for the $m = 1$ levels. The expected strongest ZOB state is indicated in bold, and these couplings are expected to be the strongest, since they have $\Delta\nu \leq 3$, and $\Delta m \leq 3$,

$$\begin{aligned} a_2' \text{ symmetry: } & 16^1 23^1 m^0 \dots \mathbf{11^1 m^0}, \\ a_2'' \text{ symmetry: } & 9^1 16^1 m^0 \dots \mathbf{13^1 m^0} \dots 12^1 24^1 m^0. \end{aligned}$$

We have omitted $12^1 15^1 m^{0,1}$ from the possible interactions above, since $12^1 15^1$ has b_2 symmetry, and hence, its $m = 0$ level cannot interact with the $m = 0$ level of either 13^1 or 11^1 , but the $m = 1$ level could be interacting with $13^1 m^1$. Moreover, being a combination band, this transition is not expected to be inherently intense, but we cannot completely rule out a minor contribution to the REMPI feature. The ZEKE band is expected at 1006 cm^{-1} , and since only a very weak band is seen at this wavenumber, we conclude that any involvement is minimal.

In previous ZEKE studies of vibrational and vibtor studies in *p*-fluorotoluene,^{27,43} we have found that the low-energy region can often give a good guide as to the contributing levels. Hence, we highlight that the ZEKE spectra recorded here, via the low-wavenumber side of the $800\text{--}850\text{ cm}^{-1}$ REMPI feature, show various torsional and

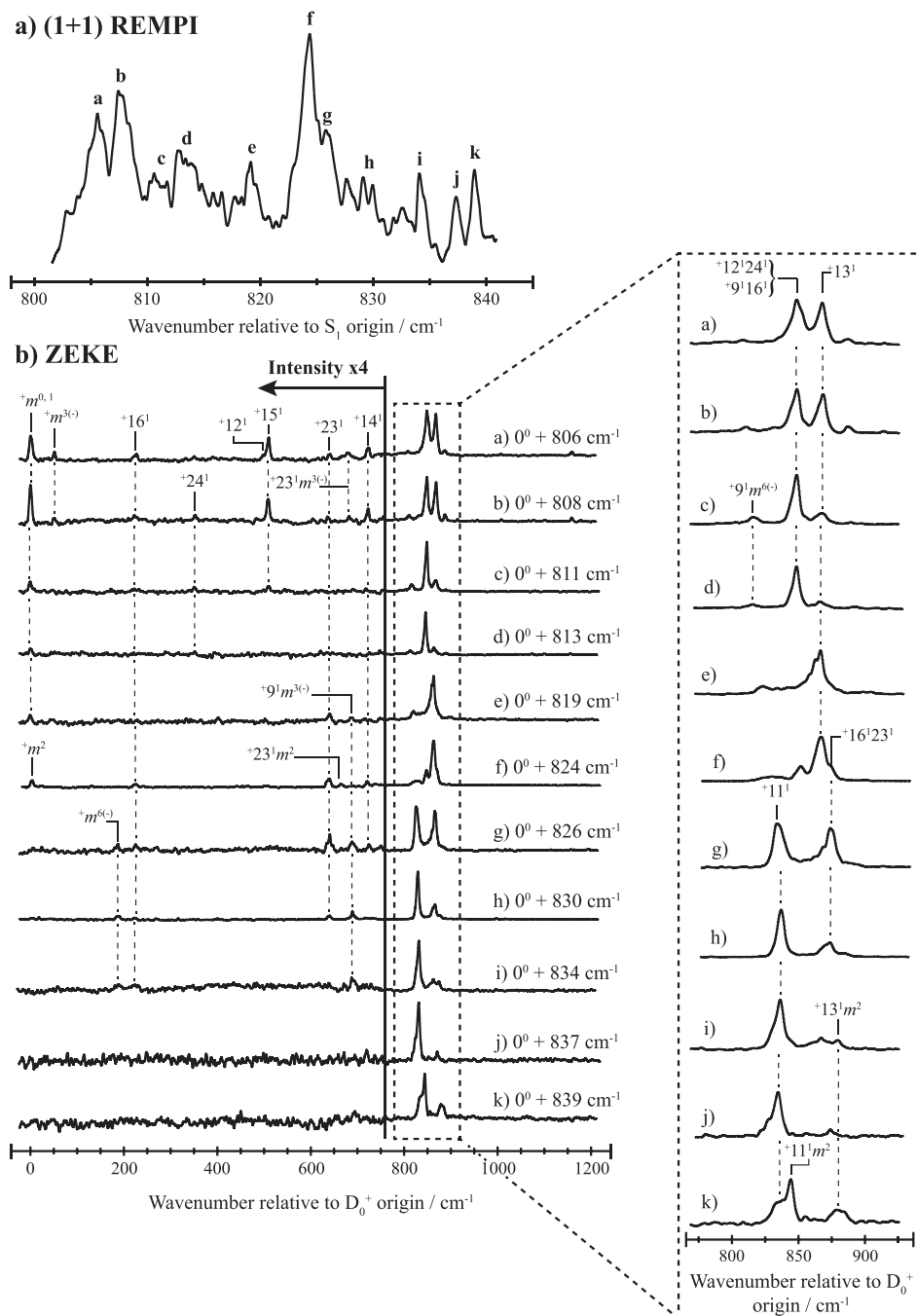


FIG. 12. ZEKE spectra recorded at the indicated positions within the 800–850 cm^{-1} feature in the (1 + 1) REMPI spectrum, with the relevant section shown at the top of the figure. The intensity of the first $\sim 750 \text{ cm}^{-1}$ has been enhanced by $\times 4$ to emphasize the low-wavenumber bands. Expansions of the 750–950 cm^{-1} regions of the ZEKE spectra are shown in the side panel on the right. Assignments are indicated by the main zero-order state expected to be contributing to each of the main features. The activity is consistent with vibronic coupling combined with interactions between different zero-order states (see text for further discussion).

fundamental bands. Recall that when we excited via 16^1 , then both $+m^{0,1}$ and $+16^1$ bands were seen in the ZEKE spectrum (Fig. 7). As such, we conclude that the observation of these bands is consistent with the involvement of the a_2'' symmetry $9^1 16^1$. Similarly, weak $+12^1$, $+23^1$, and $+24^1$ bands are also seen when exciting on the low-wavenumber side of the 800–850 cm^{-1} REMPI feature, consistent with involvement of $12^1 24^1$. The expected positions of the ZEKE

bands from these two combination bands are coincident at 849 cm^{-1} and so consistent with the lower of the two intense bands seen at the lower excitation wavenumbers. The higher-wavenumber band is consistent with $+13^1$. Hence, we conclude that in this wavenumber region of the S_1 state, we have significant contributions from three eigenstates arising from interactions involving 13^1 , $9^1 16^1$, and $12^1 24^1$, with the interactions between the 13^1 ZOB state and each

TABLE III. Expected wavenumbers of S_1 zero-order states that could contribute to the 800–850 cm^{-1} feature in the $(1+1)$ REMPI spectrum.

Level ^{a,b}		Symmetry ^c		State	
$m = 0$	$m = 1$	$m = 0$	$m = 1$	S_1^d	D_0^{+d}
		$G_{12} (C_{2v})$	G_{12}		
13¹					
$12^1 24^1 m^0$	$12^1 24^1 m^1$	$a_2''(b_1)$	e'	815	849
$9^1 16^1 m^0$	$9^1 16^1 m^1$	$a_2''(b_1)$	e'	819	849
	$24^2 m^5$		e''	822	831
$13^1 m^0$	$13^1 m^1$	$a_2''(b_1)$	e'	824	861
	$15^2 m^4$		e'	820	1097
$12^1 16^1 m^{6(-)}$		a_2''		843	911
$12^1 15^1 m^{0e}$	$12^1 15^1 m^{1e}$	$a_1''(b_2)$	e'	838	1006
	$11^1 m^2$		e'	846	846
$23^1 m^{6(-)}$		a_2''		835	829
11¹					
$9^1 m^{6(-)}$		a_2'		826	822
	$14^1 m^5$		e'	805	849
$16^1 23^1 m^0$	$16^1 23^1 m^1$	$a_2'(a_2)$	e''	828	856
	$12^1 24^1 m^2$		e''	831	865
$11^1 m^0$	$11^1 m^1$	$a_2'(a_2)$	e''	830	830
	$9^1 16^1 m^2$		e''	835	865
	$13^1 m^2$		e''	840	877
	$15^1 24^1 m^5$		e''	845	988
	$16^1 23^1 m^2$		e'	844	872
$12^1 24^1 m^{3(+)}$		a_2'		859	894

^aThe levels have been separated into those vibronically accessible from the $m = 0$ and $m = 1$ levels of the S_0 zero-point vibrational level, which can interact either with the $m = 0$ or $m = 1$ level of the expected zero-order bright states, 13^1 and 11^1 (see text for further commentary).

^bWithin each block, levels are given in the expected wavenumber order for the S_1 state, although interactions between the zero-order states could change the ordering.

^cSymmetries of the levels accessible from the indicated $m = 0$ or $m = 1$ levels. C_{2v} symmetry labels are given for the pyrrolyl ring lying in the yz -plane. For levels where both $m = 0$ and $m = 1$ are possible, both the C_{2v} label for the vibration and the two corresponding G_{12} symmetry labels are given. For other vibron levels, just the G_{12} label is given.

^dThese are calculated using experimental vibrational values, where they exist, or using a calculated value, where they do not (see Table II). For corresponding $m = 0$ and $m = 1$ levels, the same value applies, under the assumption that there are no interactions between levels. (The given values have been adjusted to be relative to the appropriate $+m^0$ or $+m^1$ scale.) The torsional energies were obtained from the V_6 and F parameters reported in Ref. 20.

^eThe $12^1 15^1 m^1$ level could interact with $13^1 m^1$, but the $12^1 15^1 m^0$ state cannot interact with $13^1 m^0$, as it has a different symmetry. The $12^1 15^1 m^0$ state could be vibronically active but, being a combination band, is unlikely to be very intense.

of the combinations ($\Delta v = 3$) expected to be stronger than those between the two combinations ($\Delta v = 4$); it appears that the $9^1 16^1$ interaction with 13^1 is the stronger. From the lower-wavenumber activity, based upon relative intensities, we can also deduce that there is more $9^1 16^1$ character at the very start of the feature, with $12^1 24^1$ then in the ascendent, before the 13^1 contribution becomes dominant at $\sim 824 \text{ cm}^{-1}$.

From 824 cm^{-1} onwards, we also see activity from $+23^1$ and $+16^1$ reappearing when exciting in the center of the REMPI feature, where $16^1 23^1$ is expected. We also see that the band at $\sim 860 \text{ cm}^{-1}$ becomes more complicated in structure, consistent with overlapping $+13^1$ and $+16^1 23^1$ contributions. To slightly higher wavenumbers, $+13^1$ is expected to wane in intensity, while $+16^1 23^1$ waxes, and the ZEKE spectra confirm this, with the strongest contribution from $+23^1$ bands in the $824\text{--}830 \text{ cm}^{-1}$ excitation region. We also see a ZEKE band at $\sim 830 \text{ cm}^{-1}$, assigned to $+11^1$, which appears in the ZEKE spectra from $0^0 + 826 \text{ cm}^{-1}$ —slightly broadened in that spectrum and then as a narrower band in the spectrum recorded at $0^0 + 830 \text{ cm}^{-1}$. These observations confirm contributions from eigenstates made up predominantly from 11^1 and $16^1 23^1$ to the mid- to high-wavenumber end of the $800\text{--}850 \text{ cm}^{-1}$ feature.

Various other bands can also be seen, some of which may be related to FC activity, but we highlight that there are strong indications that there is a contribution from $9^1 m^{6(-)}$ to the low-wavenumber end of the feature, expected to interact with $11^1 m^0$. In addition, at the high-wavenumber end of the feature, there are contributions from $13^1 m^2$, via interaction with $11^1 m^1$ and $11^1 m^2$ via interaction with $13^1 m^1$. It is difficult to be definitive about other contributions to the $800\text{--}850 \text{ cm}^{-1}$ feature, but it is likely that smaller, higher-order interactions are occurring, involving other levels indicated in Table III.

Generally, the discussed interactions appear to give a good correspondence to the observed features seen in the ZEKE spectra (see Fig. 12). On the expanded traces on the right-hand side of Fig. 12, we have indicated the expected positions of the dominant contributions, noting that the eigenstates will be linear combinations of each ZOB state with the coupled ZOD states of the same symmetry. The low-wavenumber side of the REMPI band appears to arise mostly from the transitions involving eigenstates with $13^1 m^{0,1}$ contributions, while the high-wavenumber side mostly comprises those with $11^1 m^{0,1}$. The ZEKE spectra clearly indicate that a number of contributions are present and that the REMPI feature therefore comprises transitions to a number of resulting eigenstates. Importantly, a number of these involve vibron levels that can only interact with one of the two m levels associated with a particular ZOB state. Overall, it means that within this narrow range, four possible independent routes for energy delocalization can occur. This is reminiscent of a feature seen in the REMPI spectrum of *p*-fluorotoluene, where independent energy delocalization routes of a different symmetry were also identified.⁴³

In summary, this is an unusually rich region of the spectrum and arises from the serendipitous location of (at least) two vibronically allowed ZOBs, each with $m = 0$ and $m = 1$ components, which happen to interact strongly with several vibrational and/or vibron levels. It is notable that this feature is the only one in the REMPI spectrum, in the region scanned, which shows such a complicated structure, although we commented on the likelihood of some interactions in the $630\text{--}720 \text{ cm}^{-1}$ region (see Sec. III G 6).

9. ZEKE spectra via the $>900 \text{ cm}^{-1}$ features

To higher wavenumbers, a few other weaker features appear in the REMPI spectrum, which are absent from the LIF spectrum

(see Fig. 1). We have recorded ZEKE spectra via these, which are shown in Fig. 13. In each case, there is a single intense $\Delta\nu = 0$ band consistent with our expectations of largely diagonal FCFs and reminiscent of the ZEKE spectra via 24^1 and 12^1 ; together with the calculated values in Table II, this allows the assignments to be made, as shown in Fig. 13. The REMPI band at 907 cm^{-1} is assigned to the remaining a_2 symmetry vibration, 10^1 , with the 971 cm^{-1} band being assigned to a third b_2 symmetry vibration, 22^1 . Both of these provide good agreement with the calculated wavenumbers of the vibrations in the S_1 state and cation and have symmetries consistent with the vibronic coupling mechanisms discussed; they both agree with suggested assignments in Ref. 11. The assignment of the weak structure above the $\Delta\nu = 0$ band in the 22^1 ZEKE spectrum is unclear.

There is no obvious pyrrolyl-ring localized fundamental of the correct symmetry to assign the band at 1100 cm^{-1} . Interestingly, this band is not apparent in the $(1 + 1)$ REMPI spectrum reported in the picosecond study,¹¹ and indeed, there seem to be more transitions at these higher wavenumbers, than apparent in our nanosecond spectrum, which may be linked to distinct lifetime behaviors of the different levels.

An assignment of the 1100 cm^{-1} REMPI band to 7^1 is discounted: it would be the only a_1 symmetry fundamental to be active in the one-photon spectrum and is symmetry forbidden; moreover, this transition is observed to slightly lower wavenumbers in the $(2 + 2)$ REMPI spectrum (see Fig. 2, Table II, and Ref. 11). Although a possible assignment to the $9^1 12^1$ combination would be consistent with the excitation wavenumber, this is not consistent with the wavenumber of the corresponding ZEKE band, with the

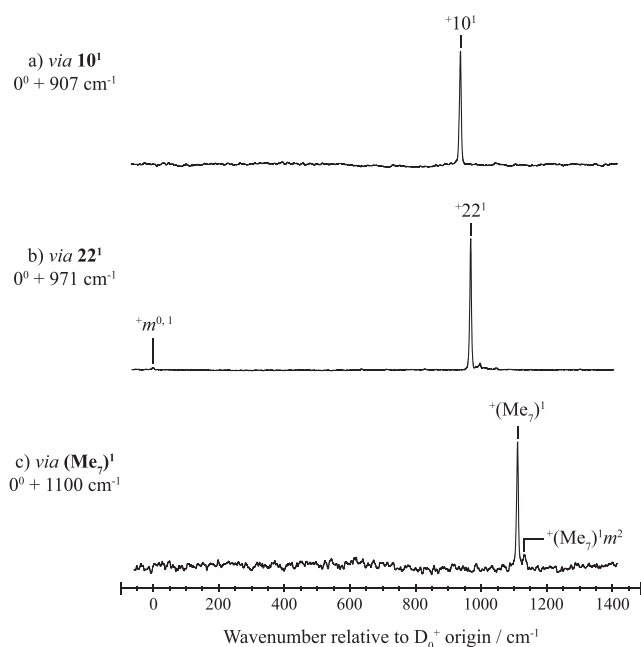


FIG. 13. ZEKE spectra via the three bands that appear in the $>900\text{ cm}^{-1}$ region of the $(1 + 1)$ REMPI spectrum, with suggested assignments.

$^{+12^1}$ wavenumber established in Sec. III G 7 and $^{+9^1}$ established in Sec. III G 6. We also reject $6^1 m^{3(-)}$ as it would be the only vibtor transition in this region, which is out of line with the torsional structure seen on the origin (see Fig. 1 and Ref. 20) and the vibtor structure associated with 9^1 (see Sec. III G 6). We finally opt for a transition to a methyl-localized vibration, Me_7 , which corresponds to an in-plane rock of the methyl group³³ and would fit with the changing dispersion interactions experienced by the methyl group in the S_0 and S_1 electronic states, consistent with the change in torsional potential between those two states.^{16,20}

IV. DISCUSSION

A. Vibrations

1. Vibrations in S_0

The ground state IR and Raman data, obtained from liquid, solution, and surface studies,^{23,24} were discussed in Ref. 33 and are presented in Table II; in Ref. 33, we also presented calculated S_0 values (B3LYP/aug-cc-pVTZ, scaled by 0.97), which were in very good agreement with the experimental values, and we also discussed previously reported calculated values. We only include our calculated values in Table II, as there was good agreement between the various calculated values, once scaling had been considered. In Table II, we have tabulated the results from the DF study of Biswas *et al.*¹⁸ alongside those obtained in the present work. For the cases where a value was obtained in both studies, the values are in good agreement with each other and with the present calculated values. A couple of the assignments in Ref. 18 appear ambiguous, for example, the value for P_{20} has an alternative assignment to Me_6 , the methyl umbrella mode. The assignment of a 1100 cm^{-1} vibration could be assigned to either Me_7 or Me_8 .

The present study obtains a number of jet-cooled, gas-phase S_0 vibrational wavenumber values for the first time, which are also in generally good agreement with the previous IR/Raman and calculated values.

2. Vibrations in D_0^+

The wavenumbers for the D_0^+ state of the cation derived from the ZEKE spectra are given in Table II and are the first time any of these values have been reported. (No vibrational structure was reported for the conventional photoelectron spectrum of NMP by Baker *et al.*⁴⁴) The agreement between the calculated and experimental values is exceptionally good, similar to the good agreement seen for the S_0 state, and provides further confidence that the assignments are correct. Of course, the vibrational wavenumbers for the cation are expected to be similar to those of Rydberg states of NMP, and we shall comment on this further in Sec. IV A 3. We provide further commentary on the activity in the ZEKE spectra in Sec. IV A 4. Cooper *et al.*¹⁵ provided some vibrational wavenumbers associated with various Rydberg states of NMP, but although some of these are close to cation values presented in Table II, the assignment of all of these is uncertain.

3. Vibrations in S_1 and vibronic coupling

We have collected the present calculated (TD-B3LYP/aug-cc-pVTZ, scaled by 0.97) and experimental values for the wavenumbers

of the S_1 state vibrations together in Table II. Also included are the (TD-B3LYP/aug-cc-pVDZ) calculated values reported in Ref. 11, together with calculated values (CIS/6-31G**) reported in Ref. 19. (We have only included the calculated values from both Refs. 11 and 19 that were included in Ref. 11 and where they were assigned to particular vibrations.) Although the TD-B3LYP/aug-cc-pVDZ and TD-B3LYP/aug-cc-pVTZ results of Ref. 11 and the present work are in close agreement (noting that the former do not appear to have been scaled), there is some disagreement with the CIS/6-31G** values of Ref. 19. Since the S_1 state is Rydberg-like close to the FC region, then we would expect the vibrational wavenumbers for S_1 to be similar to those in the D_0^+ state. Indeed, if the present *calculated* values in Table II are considered, this is indeed the case, with all calculated S_1 vibrational wavenumbers being very close to the corresponding D_0^+ ones for all symmetries, although the wavenumbers of the a_2 symmetry vibrations are slightly more discrepant. Overall, therefore, coupled with the good agreement between the experimental and calculated D_0^+ vibrational wavenumbers, we have more confidence in the TD-B3LYP calculated wavenumbers for the S_1 state than the CIS ones of Ref. 19.

In Fig. 14(a), it may be seen that the calculated vibrational motions of the S_1 state are similar to those in the S_0 state, supporting the use of the same P_i labels for both states, and in Ref. 33, it was shown that similar comments apply to the vibrations of the D_0^+ state. In addition, the $D_0^+ \leftarrow S_1$ Duschinsky matrix shown in Fig. 14(b) is highly diagonal, showing that the calculated vibrational motions in the S_1 state are almost identical to those in the cation, as expected for a Rydberg state with the corresponding ionic core. Given that there is very good agreement between the calculated vibrational wavenumbers for the D_0^+ state and the obtained experimental values (Table II), then we would also expect correspondingly close agreement for the S_1 vibrations. It is noteworthy although this expectation is met for the in-plane a_1 and b_2 vibrations, there are significant differences between the calculated and experimental S_1 vibrational wavenumbers for the out-of-plane b_1 and a_2 vibrations, with the S_1 experimental values all being significantly lower, particularly for P_{15} . We now comment on these observations in the light of the known vibronic interactions in this molecule.

In Fig. 3, we have indicated the approximate vertical energetic locations of the various excited states of NMP, i.e., at the geometry of the \bar{X} state. The NMP molecule is unusual in two key related aspects: first, in the FC region, its first excited state is Rydberg in character, S_1 ($a_2, 3s$), yet it fluoresces; and second, there are closely lying states of three different symmetries that each allow distinct vibronic interactions to be induced. In Fig. 3, we have indicated the main excited electronic character of each state and its symmetry, as well as the symmetries of the vibrations that induce the vibronic coupling for each nearby electronic state; furthermore, the calculated oscillator strengths are also indicated, since for intensity to be stolen via vibronic coupling, there must be something to be stolen. Some of the calculated oscillator strengths for some of the A_2 electronic states are not zero (indicated by an “*” in Fig. 3). This is likely because at the potential minimum of the \bar{X} state of NMP, the geometry is C_s as opposed to C_{2v} , and this breakdown of C_{2v} symmetry means that these states can be calculated as weakly allowed.

It is clear from the assignments of the different spectra that there is strong vibronic coupling induced by vibrations of both b_1

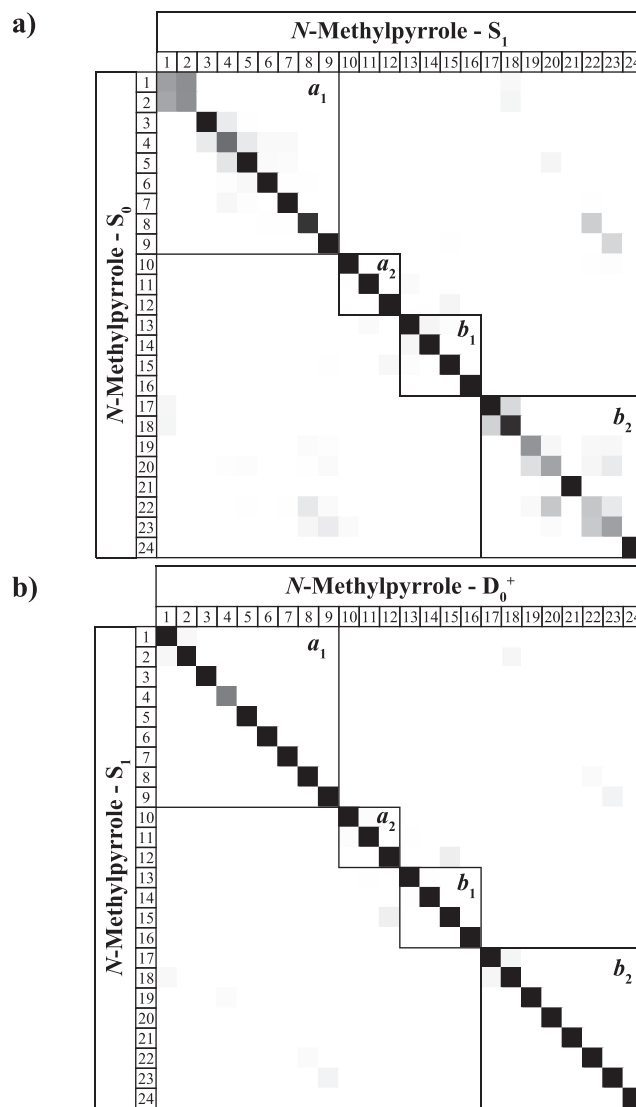


FIG. 14. Duschinsky matrices for the (a) $S_0 \leftrightarrow S_1$, and (b) $S_1 \leftrightarrow D_0^+$ transitions. The depth of shading represents the coefficients of mixing between vibrations in the two electronic states between 0 (white) and 1 (black). The S_1 vibrations can, for the most part, be seen to be dominated by a single S_0 vibration, allowing the P_i labels to be used for those vibrations. The D_0^+ vibrations are calculated to be almost identical to those of the S_1 state; however, the experimental results suggest that some of the S_1 vibrations are affected by vibronic coupling. In Ref. 33, we also discussed the vibrations of D_0^+ expressed in terms of those of the S_0 state.

and b_2 symmetries. Indeed, all four b_1 vibrations are observed in the REMPI spectrum, as well as the three lowest wavenumber b_2 vibrations (with the others being higher in wavenumber than the region scanned.) The intensity of the b_2 symmetry, 23^1 transition is significant, as are the b_1 symmetry 16^1 and 15^1 bands; some caution is required with the intensities, however, since the lifetimes of the levels are decreasing with the increasing wavenumber, albeit not monotonically.¹¹ Weaker, but still significant are transitions involving all

three a_2 symmetry vibrations. Our resolution is sufficient to discern the rotational band profile type, and we show these in Fig. S1 of the [supplementary material](#) for the 16^1 , 15^1 , and 23^1 bands. These profiles are as expected,³⁸ being of type b for 16^1 and 15^1 , which gains intensity from the $(a_2, 3p_x) ^1B_2 \leftarrow S_0$ transition, and type c for 23^1 , which gains intensity from the $(a_2, 3p_y) ^1B_1 \leftarrow S_0$ transition. Bands corresponding to transitions to a_2 symmetry vibrations are expected to show type a band profiles, and this is consistent with observations. We find that our REMPI spectra appear to be slightly rotationally colder than our LIF spectra and that we only see some bands clearly in the REMPI spectra; when observed, the band profiles are clearer and slightly wider in the rotationally warmer LIF spectra.

As expected, we see no transitions that involve totally symmetric vibrations in our $(1 + 1)$ REMPI spectrum, since these are forbidden in one-photon transitions, although such transitions are allowed and dominate in the $(2 + 2)$ REMPI spectrum, as can be seen in the spectrum in Fig. 2 and that presented in Ref. 11. The bands in the $(2 + 2)$ REMPI spectrum are broader than those of the $(1 + 1)$ REMPI spectra, likely due to power broadening effects; the bands in the present $(2 + 2)$ REMPI spectrum in Fig. 2 are significantly narrower than those in the corresponding spectrum in Ref. 11, in line with the higher power and pulse width of the picosecond laser employed. Despite the rapidly decreasing lifetimes of the levels,¹¹ no broadening is evident in the $(1 + 1)$ REMPI spectra, for all bands that we have recorded, up to $\sim 1110 \text{ cm}^{-1}$ (see Fig. 1)—consistent with lifetime broadening effects not being significant, in line with the lifetimes cited in Ref. 11.

From the assignments, the $(1 + 1)$ REMPI and LIF spectra display three distinct vibronic coupling mechanisms, with the $(2 + 2)$ REMPI spectrum dominated by FC activity—indeed, no evidence of vibronic coupling is seen in the $(2 + 2)$ REMPI spectrum, although it still can occur. As well as being responsible for the observed intensities in absorption, these vibronic coupling mechanisms will also operate for the emissions and are consistent with the DF and 2D-LIF spectra. As remarked in Sec. III E, the vibrational structure seen will depend upon the symmetry of the level from which emission occurs. The assignment of the DF spectra indicate that the P_{15} vibration is the main inducing mode for the emission, with the strongest band always arising from a combination of P_{15} with the corresponding intermediate S_1 vibrational level. In addition, we also see vibronic activity associated with the other b_1 symmetry vibrations, with this being quite strong also for P_{16} , as well as some b_2 and, to a lesser extent, a_2 vibrations, confirming that the same vibronic mechanisms are operating in both emission and absorption. Although the 16^1 , 15^1 , 23^1 , and 14^1 transitions are strong in absorption, with some caution required when considering the intensities of the REMPI and LIF bands because of the lifetime variation, the vibronic coupling involving P_{15} demonstrates by far the strongest bands in emission.

As commented hereinbefore, we expect the S_1 and D_0^+ wavenumbers to be very similar for each vibration, since the S_1 state is Rydberg-like, and this expectation is borne out in the calculated wavenumbers, for the most part, and by the corresponding almost perfectly diagonal Duschinsky matrix in Fig. 14(b). This is consistent with the highly diagonal nature of the FCFs for the ionization, as observed for almost all vibrations. The two major exceptions are first in the ZEKE spectrum via 16^1 , where the origin transition is

clearly seen, and in the ZEKE spectrum via 15^1 , where we see both the origin band and a sizeable $^+16^1$ band. We have commented in Sec. III G 4 regarding the absence or relative weakness of $^+15^1$ ZEKE bands in both of these spectra but also the significant step in the PIE curve when exciting via $^+15^1$ —these points are the subject of ongoing investigations.⁴² Here, we will discuss the effect of vibronic coupling in the S_1 state.

Often, two types vibronic effects are described: a dependence of the electronic transition moment on the nuclear coordinates and intensity stealing via vibronic interactions. In the book authored by Bunker and Jensen,³⁰ it is concluded that these are two manifestations of the Herzberg–Teller effect and can be viewed as vibration-induced mixing of electronic wavefunctions away from the equilibrium position. Hence, for a one-photon forbidden absorption, if we denote the final electronic state of symmetry, i , in a transition by $\Phi'_{e,i}(0')$, where $0'$ represents the equilibrium geometry of that state, then for small deviations, δQ_j , along one or more normal modes of symmetry j , then we can express the electronic wavefunction of the excited state at the slightly distorted geometry as

$$\Phi'_{e,i}(\delta Q_j) = c_i \Phi'_{e,i}(0') + \sum_j c_j \Phi_{e,j}(0'), \quad (6)$$

where the $\Phi_{e,j}$ are electronic wavefunctions of other excited states of symmetry j . For small displacements, we can ignore anharmonic effects and $|c_j|$ will be small and then vanish when all $\delta Q_j = 0$; additionally, $|c_i|$ will be close to, but less than, 1 for $\delta Q_j \neq 0$ and equal to 1 when $\delta Q_j = 0$. Assuming that c_j are proportional to the normal coordinate displacements,³⁰ then

$$\Phi'_{e,i}(\delta Q_j) = c_i \Phi'_{e,i}(0') + \sum_j C_j Q_j \Phi_{e,j}(0'). \quad (7)$$

Thus, the electronic potential experienced by the molecule will vary along a normal coordinate (more generally, one of the nuclear coordinates could be torsion), and resultant mixings are possible, i.e., C_j is non-zero when the symmetry, j , is such that vibronic coupling occurs during a transition from the ground electronic state. It is this variation that can be viewed as mixing in of other excited state characters of symmetry j , as a result of a vibronic interaction, away from the equilibrium position of $\Phi'_{e,i}$. Similar arguments apply to emission, although in jet-cooled experiments the emitting state will often be a vibrationally excited level of the upper electronic state; the latter will also be true of the intermediate level employed for the resonant ZEKE transitions.

We have seen that there is good agreement between the calculated b_1 symmetry vibrational wavenumbers for the S_1 state and the cation and also between the calculated and experimental values for the cation; in contrast, we find significantly lower values for the experimental S_1 b_1 symmetry vibrations. Taken together, these observations strongly suggest in the S_1 state, vibronic coupling changes the potential experienced by the molecule along the b_1 coordinates and leads to the observed lowering of those vibrational wavenumbers. A similar, although less marked, scenario emerges for the a_2 symmetry vibrations also. It is extremely interesting that although the in-plane b_2 symmetry vibrations are also involved in inducing vibronic coupling, the experimental values for the three observed vibrations are almost identical in the S_1 and

D_0^+ states, and so, apparently, no potential distortion occurs along those coordinates.

4. ZEKE spectra

Considering the ZEKE spectra further, we have highlighted that the majority exhibit very diagonal FCFs, with the Δm , $\Delta \nu$, or $\Delta(\nu, m) = 0$ band being by far the most intense in the spectrum—the ZEKE spectra recorded via the torsional levels have been discussed in Ref. 20. The main exceptions to this are the ZEKE spectra recorded via the S_1 14^1 , 15^1 , and 16^1 levels (see Fig. 7), where the origin band appears, which we shall now discuss.

We first comment that the ZEKE spectrum recorded via 14^1 is very much as expected, with very strong diagonal FCF character but with a weak origin band. (The excitation will involve both $m = 0$ and $m = 1$ components, and so the dominant feature is expected to be the overlapped $^{+14^1}m^{0,1}$ bands; this will be the case for other intermediates vibrational levels also.) The ZEKE spectrum recorded via the much stronger 16^1 level, although being dominated by the $^{+16^1}$ band, also exhibits a sizeable origin band, as well as a number of weak torsional bands, and the ZEKE spectrum via $^{+15^1}$ also exhibits a strong origin band, as well as a $^{+16^1}$ band, with the weakness of the $\Delta \nu = 0$ ZEKE band commented on in Sec. III G 4.

We have seen that vibronic interactions can cause a change in the potential along coordinates corresponding to vibronic-coupling inducing vibrations, and such a vibrationally excited level could have a slightly distorted average geometry. For b_1 vibrations, this would lead to a small distortion to an out-of-plane averaged geometry and would lead to a C_s symmetry molecule, with the reflection plane being xz in the current axis system; then, the b_1 (a_2'') and a_1 (a_1') symmetry levels become totally symmetric in the C_s point group. Thus, the origin band in the ZEKE spectrum would become weakly allowed via these intermediate levels, as seen, and similarly for the $^{+24^1}m^{3(+)}$ band via 15^1 . Such a mechanism would also lead to e'' symmetry torsional and vibtor levels also becoming allowed, with e' levels already being symmetry allowed from the $m = 1$ levels associated with the b_1 symmetry intermediate vibrational levels. Thus, this is a possible explanation for the appearance of the various torsional bands, particularly evident in the 15^1 and 16^1 ZEKE spectra. That these bands are relatively weak would be in line with the only small geometric distortions expected.

Although symmetry-forbidden bands are prevalent in photoelectron and ZEKE spectra, their origin is not always clear, with the intrachannel-coupling mechanism of Rathbone *et al.*⁴⁵ for photoelectron spectroscopy (PES), extended to Rydberg states and ZEKE spectroscopy,⁴⁶ being one such mechanism. In outline, the outgoing photoelectron wave (in PES) or the high- n Rydberg electron (in ZEKE) can interact with the vibrations (or torsions and vibtor levels) of the cation core. For NMP, the $np \leftarrow 3s$ excitations are most likely (being $\Delta l = 1$ from the $3s$ S_1 Rydberg state), with these having the symmetries b_1 for np_x , b_2 for np_y , and a_1 for np_z . Thus, vibrational bands in the ZEKE spectra corresponding to these symmetries, particularly low-frequency, high-amplitude vibrations, can be rationalized by this mechanism.

We now come back to the ZEKE spectrum via 15^1 , which has very unexpected activity. First, it is the only ZEKE spectrum

recorded for NMP that does not have the dominant $\Delta \nu = 0$, or equivalent, band; however, the PIE spectrum suggests that this absence is due to some interaction occurring in the cation (Fig. 7 and Sec. III G 4), which is under further investigation.⁴² Here, we comment on the appearance of the $^{+16^1}$ band in this ZEKE spectrum, despite the Duschinsky matrices (Fig. 14) indicating that any mixing between vibrational modes during the ionization is minimal. Earlier, in the present section, we have suggested the possibility that the S_1 potential is affected by the vibronic coupling along the out-of-plane coordinates, particularly those of b_1 symmetry, and this would not be reflected in the calculated Duschinsky matrices; on the other hand, the DF spectra are clear that the intermediate levels are dominated by the expected vibration but indicate that there is cross-activity in the DF spectra recorded via 16^1 and 15^1 (see Figs. 4 and 5). We propose that there is indeed some Duschinsky-type mixing between the 16^1 and 15^1 modes, caused by the vibronically induced change in the S_1 wavefunctions away from their cation-like form, therefore leading to off-diagonal FC activity in both the ZEKE and DF spectra via 15^1 and in the DF spectrum via 16^1 ; this would not be evident in the calculated Duschinsky matrices. With this in mind, we might therefore expect to have seen $^{+15^1}$ activity in the ZEKE spectrum recorded via 16^1 ; however, as we commented on in Sec. III G 4, there is a precipitous drop-off in photoionization cross section of all PIEs recorded to higher wavenumbers, as shown in Fig. 7, followed by further multiphoton activity (not shown and which will be reported at a later date⁴²).

B. Comments on photodynamics

The prevalence of the pyrrolyl ring in biomolecules, and the importance of the photostability of biomolecules, has naturally led to the simplest molecules that contain this group, pyrroles and substituted pyrroles, being the targets for photodynamical studies. Of interest is the effect of substituting the N-bonded H atom in pyrrole for a methyl group. It is known that in the S_1 state, pyrrole rapidly loses the N-bound H atom and is presumed to form the pyrrolyl radical and an H atom.^{12,21} By analogy, NMP has been suggested to lose a methyl group and also form the pyrrolyl radical.⁵ Understanding both how electronically excited molecules fragment and how they efficiently delocalize their energy is the key aspect of understanding the biophysics underpinning solar-radiation-induced radical production, which can lead to cancer formation in living organisms.

As commented on in the above, the first electronically excited state of NMP is Rydberg-like close to the FC region, but at the long range, this state evolves into a σ^* unbound state along the N-CH₃ coordinate. Furthermore, movement along this coordinate involves significant structural changes, mainly involving the CH₃ group evolving from a pyramidal to planar geometry. In Fig. 15, we have optimized the geometry of the S_0 state of NMP at the CAM-B3LYP/aug-cc-pVTZ level and then calculated the vertical excitation energies of excited states at a range of N-CH₃ bond lengths, constraining the rest of the geometric parameters. These plots look similar to those in Ref. 9, and as may be seen, there is a significant barrier to dissociation. We have also optimized the geometries of the ground electronic states of the pyrrolyl radical (\tilde{X}^2A_2) and the CH₃ radical (\tilde{X}^2A_2'') and indicated the energy of this dissociation asymptote in Fig. 15; this confirms that the asymptote of the

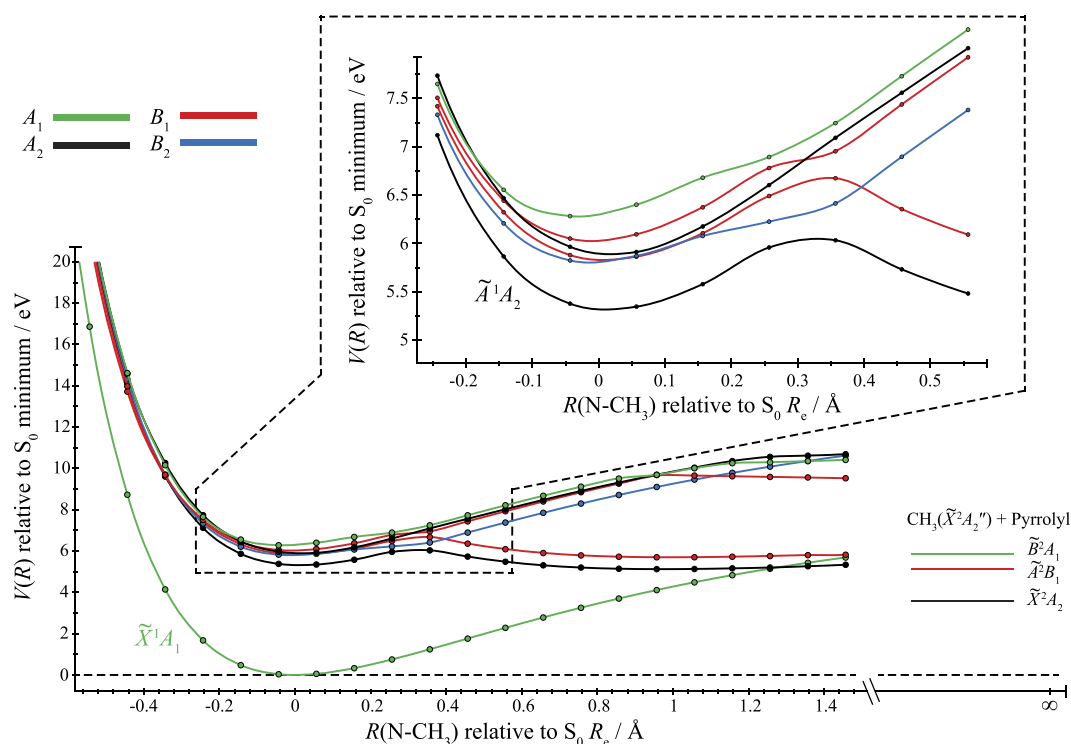


FIG. 15. Calculated, constrained potential energy plots for the ground and lowest six electronically excited states of NMP. TD-CAM-B3LYP/aug-cc-pVTZ level calculations were performed, with the geometry fixed at that optimized for the \tilde{X} state, except for varying the N-CH₃ bond length. Vertical excitation energies were calculated at a range of N-CH₃ bond lengths for these states to produce the curves shown. In the top right of the figure, an expanded view of the region close to the minima of the excited states is shown. The colors represent the symmetries of the electronic states, as shown in the legend (see also Fig. 3 and text). On the bottom right of the diagram, the lowest three pyrrrolyl + CH₃ asymptotes are shown. Their energies are obtained by optimizing the geometries of the ground states of the two radicals and then calculating vertical excitation energies. The three lowest asymptotes are found to correspond to ground state CH₃, together with three electronic states of pyrrrolyl. The coloring indicates the symmetry of the NMP state that correlates with each asymptote. The lowest dissociation asymptote lies significantly below the minimum of the S₁ (1A_2) state, consistent with results from photodissociation experiments; relaxed geometry scans would allow these asymptotes to join smoothly to the respective minima.

constrained S₁ state is far above the “relaxed” asymptote, with the latter lying below the minimum of the S₁ state, in agreement with photodissociation studies.^{5,9,11} The optimized geometries of the pyrrrolyl and methyl radicals are given in Fig. S2 of the [supplementary material](#); both ground states are found to be planar, with the geometric parameters of pyrrrolyl agreeing well with those of Gianola *et al.*⁴⁷ Although there are issues with the calculated state ordering in Ref. 8, the relaxed scan shown in Fig. 3 of that work indicates that a barrier still exists to dissociation in the S₁ state. In Fig. 15, we have also indicated the positions of the next two dissociation asymptotes, which involve electronically excited pyrrrolyl (the pyrrrolyl excitation energies used in Fig. 15 are CAM-B3LYP/aug-cc-pVTZ calculated vertical excitations from ground state pyrrrolyl). These lie below the asymptotes with electronically excited CH₃ (not shown), since the latter are located at >5.7 eV above its ground state.⁴⁸ It may be seen that the S₁ state of NMP correlates adiabatically with the lowest energy asymptote, pyrrrolyl (\tilde{X}^2A_2) + CH₃ (\tilde{X}^2A_2''); we assume that it correlates diabatically to an asymptote involving the 3s Rydberg state of pyrrrolyl. The S₀ state correlates with the third asymptote and so produces electronically excited

pyrrrolyl, \tilde{B}^2A_1 , and ground state CH₃. The (*a*₂, 3p_y) 1B_1 state presumably dissociates diabatically to produce the 3p_y Rydberg state of pyrrrolyl, but adiabatically it produces the first electronic state, \tilde{A}^2B_1 plus ground state CH₃.

Figure 15 also confirms that the \tilde{X} state potential crosses that of the S₁ state along the N-CH₃ coordinate; this represents a conical intersection between the S₁ and \tilde{X} state surfaces, providing a route for internal conversion (IC) between the two states; the \tilde{X} state also crosses the lowest 1B_1 surface. A key route to losing energy in electronically excited NMP (and related molecules) is via IC to the \tilde{X} state. In solution, IC (an isoenergetic process) is followed by subsequent solvent-induced collisional energy loss. If this energy cannot be lost via such mechanisms, for example, in the gas phase under low pressure conditions or in a supersonic jet, then photofragmentation might be expected. We observe that IC to the \tilde{X} state will, of course, produce highly vibrationally excited NMP molecules; although, undoubtedly, this will lead to intramolecular vibrational relaxation (IVR) in the S₀ state. As long as the molecule stays on the \tilde{X} state surface, it cannot dissociate, since dissociation on this surface would be to electronically excited pyrrrolyl (\tilde{B}^2A_1) and CH₃

(\tilde{X}^2A_2''), and this asymptote lies higher in energy than the ground state asymptote (see Fig. 15). Thus, although IC to the \tilde{X} state does represent a population loss mechanism from the S_1 state, it is not a direct route for subsequent dissociation to ground state pyrrolyl + CH_3 products.

Photodissociation can happen on the S_1 surface, but Fig. 15 shows that there would need to be efficient routes around the S_1 state barrier to access the dissociation asymptote, and this may reasonably be expected to depend upon the amount and form of the internal energy and so the molecular motion. It is also possible to envision an indirect mechanism consisting of efficient IC from S_1 to S_0 , followed by rapid IVR in S_0 , which then leads to a vibrational motion that allows favorable IC back to the S_1 state on the high- R side of the barrier, i.e., with vibrational motion excited that leads to extended vibrationally averaged N- CH_3 bond lengths. This process would be consistent with the observations of Tseng *et al.*⁶ and Woo and Kim¹¹ that there is a time delay before dissociation products are seen. The $S_1 \leftarrow S_0$ IC could thus produce NMP on the other side of the barrier with a longer N- CH_3 bond, which will facilitate unimolecular decay. This process could produce vibrationally excited pyrrolyl and/or CH_3 products, and although some excited CH_3 products have been probed,⁵ it would clearly be useful to interrogate other levels and also the pyrrolyl product.

There is very little pyrrolyl⁺ signal in the mass spectra we record throughout the range of the (1 + 1) REMPI spectrum; furthermore, when we observe the mass spectrum via a two-color process, such as when recording PIE spectra, we only see NMP⁺ ions (see Figs. S3 and S4 of the supplementary material). The absence of the two-color pyrrolyl⁺ signal is likely because the ionization energy of pyrrolyl is 9.11 eV;⁴⁹ similarly we do not see any significant CH_3^+ signal, whose ionization energy is 9.84 eV;⁵⁰ in both cases, therefore, ionization would require multiple photons. In our one-color experiments, as in Ref. 5, we do see various fragment ions, including weak pyrrolyl⁺ and CH_3^+ , and this is consistent with the mass spectra shown in Fig. 3 of Ref. 5 (albeit the traces seem to be the wrong way around with respect to the cited excitation wavelengths).

We now comment on some other aspects of the photodynamics studies.

We do not see long progressions involving vibrations that are related to N- CH_3 stretching vibrations over the regions scanned, either in the DF or ZEKE spectra, but this could be because of the limited region of the spectra scanned and that such vibrations would be in-plane. Dissociation of NMP to ground state pyrrolyl + CH_3 products on the S_1 surface will occur along the z -axis of NMP, since pyrrolyl is planar with the unpaired electron in an orbital localized on the nitrogen atom and pointing along the C_2 axis, and the ground state of CH_3 is planar with an electron located in an orbital that is oriented along the methyl C_3 axis. NMP is deduced to dissociate rapidly when in-plane a_1 and b_2 vibrations are excited,¹¹ and very recent simulations on pyrrole corroborate this observation.⁵¹ It seems clear that once the dissociation asymptote becomes accessible, then dissociation will lead to both fragments experiencing a significant impulse—consistent with the results of photodissociation studies.^{5,9,11}

Figure 15 shows that the potential of the lowest excited 1B_1 state of NMP has a similar profile as the S_1 state, but correlating to the first excited state of pyrrolyl and ground state CH_3 . This state may be playing an intermediate role in other IC processes or, indeed, may be

the terminal state, with dissociation on that surface producing electronically excited pyrrolyl. Wu *et al.*⁹ have invoked involvement of this state at higher excitation energies. There are various crossings between the lowest 1B_1 state and other states, so the IC behavior could be quite complicated. The involvement of excited states at particular excitation energies has also been commented on by others.^{5,6,10,11}

Some workers hypothesized that triplet states could be involved in the photodynamics of NMP.^{7,10} We observe that each of the open-shell singlet states in Fig. 15 (see also Fig. 3) has an associated triplet state, but since one of the unpaired electrons is in a Rydberg orbital, each of these triplet states would be expected to have potential energy curves that are largely parallel to their corresponding singlets and be close in energy and so exhibit similar behavior. If intersystem crossing (ISC) to the triplet versions of these Rydberg states occurs, we do not think this would lead to dissimilar spectroscopic and dynamical behavior. However, if triplet states are accessed where the two unpaired electrons occupy valence orbitals, this could affect the observed behavior and has been discussed by Blancafort *et al.*⁷ for a $\pi\pi^*$ triplet state of NMP.

The Woo and Kim picosecond study¹¹ appears to be the most comprehensive one to date, in which the lifetimes of many S_1 levels were probed across the internal energy range of ~ 0 –1850 cm^{-1} , with levels accessed by either one- or two-photon excitation. A clear, but non-monotonic, trend was identified of a decrease in lifetime with internal excitation energy of the S_1 state, with occasional small rises in lifetime occurring within the overall downward trend. Furthermore, some of the decay profiles could be fitted with a single time constant, while others required two or three, suggesting different pathways. In particular, IVR was mentioned as a possible explanation for this, with multiple excitations within the width of the picosecond laser being another. We agree with the possibility of the latter for some levels but cannot see that IVR will generally be significant, since the DOS is not very high below 1500 cm^{-1} (Fig. 16); this would be particularly true of levels at very low wavenumbers. However, one exception may be in the 800–850 cm^{-1} region, which was found to have a rather complicated time dependence in Ref. 11, consistent with the excitation of multiple states; the complexity of this feature and the involvement of multiple ZOSs was highlighted in Sec. III G 8.

It was commented in Ref. 11 that the derived lifetimes did not agree with previous work and suggested that this could be associated with different experimental conditions, for example, with regard to the time duration of the laser sources: clearly, very short laser pulses are more likely to excite more than one eigenstate. It is particularly intriguing that only the “fast” CH_3 fragments (with a kinetic energy of ~ 6000 cm^{-1}) were seen at 183 cm^{-1} , with a slow component (with a kinetic energy ~ 0 cm^{-1}) appearing weakly at 370 and 641 cm^{-1} ; the slow component became dominant at 806 cm^{-1} , with the faster component still sizeable; it was commented¹¹ that these observations were not wholly in agreement with those of Sage *et al.*⁵ A marked change in lifetime was reported at ~ 700 cm^{-1} ascribed to a non-radiative channel, and it was suggested that this could be the energy at which an S_1/S_n conical intersection could be occurring, but the curves in Fig. 15 seem to suggest that this is unlikely at these low energies, with the caveat that relaxed scans could alter the curves significantly. It is interesting that the “PHOFEX” signal for CH_3 in Ref. 11 decreases significantly at around this internal

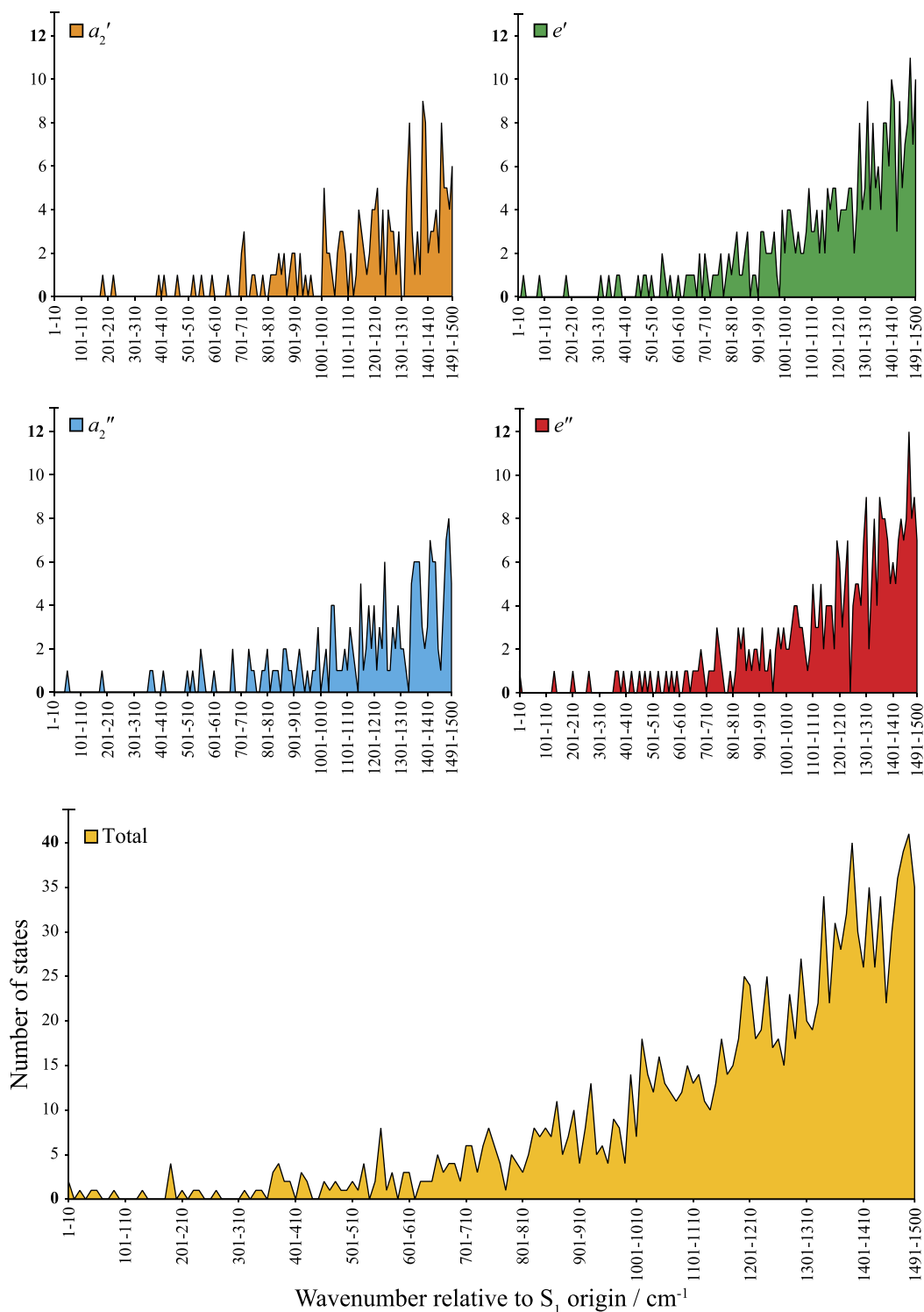


FIG. 16. Density of states (DOS) plots for NMP using calculated vibrational wavenumbers from Table II and torsional levels from Ref. 20; these correspond to the number of states within a 10 cm^{-1} wide window. (The abscissa and ordinate axis labels on the bottom plot of the figure apply to all five plots.) In the top four plots, the DOS has been broken down into the symmetries accessible from $m = 0$ and $m = 1$ of the zero-point vibrational level in the S_1 state and accessing vibrational levels of b_1 (a_2'') or b_2 (a_1'') symmetry, the symmetries of the main inducing vibrations. In the bottom plot, all symmetries are included. In all cases, torsional, vibrational, and vibtor levels have been included. It may be seen that the DOS is relatively low in the $0\text{--}1500\text{ cm}^{-1}$ region covered here, and particularly so below 1000 cm^{-1} .

energy, and it was concluded that the dissociation channel decreases in importance as other non-radiative channels open up. We suggest that one explanation for this may be that IC occurs to S_0 , followed by IVR and subsequent IC back to S_1 , but that at certain energies, it becomes more difficult for the molecule to undergo IC back to the S_1 , or perhaps to the $(a_2, 3p_y)$ 1B_1 surface, where dissociation can occur. Again, probing the pyrrolyl fragments would be a valuable addition to our knowledge of the photodynamics of this molecule.

V. CONCLUSIONS

In this work, we have presented a detailed assignment of the levels in the S_1 state of NMP based on the appearance of DF, 2D-LIF, and ZEKE spectra. Combined with previous IR and Raman data and quantum chemical calculations, the majority of assignments of the individual S_1 levels are now secure. The assignments largely agree with those of the limited levels studied by Biswas *et al.*¹⁸ as well as many of the suggested assignments put forward by Woo and Kim,¹¹ with the present work providing either concrete evidence for some of the assignments or new assignments.

We have confirmed the Rydberg nature of the S_1 state in the FC region but have suggested that some vibrationally averaged out-of-plane deviation may occur. This, and other mechanisms discussed, is a possible explanation for the appearance of various “forbidden” bands in some of the ZEKE spectra, particularly when exciting via b_1 vibrations. The main conclusion is that multiple vibronic coupling mechanisms are occurring in the S_1 state.

We find that the DOS build up is relatively slow in this molecule (Fig. 16) and the only significantly congested region of the REMPI spectrum is the 800–850 cm^{-1} region. Even in the latter case, the ZEKE spectra suggest that only limited couplings are occurring, and so this coupling falls into the restricted IVR regime, rather than statistical. Furthermore, different routes for energy delocalization occur under G_{12} symmetry. Some evidence for the involvement of the methyl rotor is seen—this is expected to drive a rapid build-up in the DOS at higher energies, as seen in *p*-fluorotoluene,^{52,53} *m*-fluorotoluene,⁵⁴ and *p*-xylene.⁵³

We have also identified highly unusual behavior following ionization via S_1 15^1 in that the expected $\Delta v = 0$ ZEKE band was surprisingly weak. The appearance of the expected large step in the PIE curve, however, indicates that this is due to unusual photoionization dynamics; this and the drop-offs in the intensities of other PIE curves are currently under further investigation.⁴²

In summary, we have confirmed, or obtained for the first time, a number of vibrational wavenumbers for the S_0 , S_1 , and D_0^+ electronic states and confirmed interactions between vibrational and torsional motion. In principle, therefore, it ought to be possible to gain detailed insight into the photodynamics of NMP, and indeed, level-specific behavior was suggested by Woo and Kim.¹¹ However, some caution is required relating to both the explicit assignments of that work, particularly as to whether only a single level was excited at particular cited wavelengths; the present study helps that assessment. For example, in the 800–850 cm^{-1} feature, it seems clear that a picosecond laser would have been exciting multiple eigenstates. The present work allows a definitive assignment of the various bands seen in the REMPI spectrum, and hence, the motion of the molecule with particular amounts of internal energy is known.

Trying to understand the wealth of photodynamic results will benefit from dynamical modeling, where particular vibrational motion is activated in the S_1 state of NMP, and the effect on the resulting photodissociation studied, as has been reported very recently for pyrrole;⁵¹ this will, of course, require reliable multidimensional potentials, particularly if multiple IC (or ISC) steps occur, as suggested herein. Overall, our results and comments emphasize the utility of knowing which eigenstates are excited in time-dependent experiments and hence reinforces the complementarity of frequency- and time-resolved experiments.

SUPPLEMENTARY MATERIAL

See the [supplementary material](#) for correlation between the P_i labels and those of Biswas *et al.*;¹⁸ band profiles of the 16^1 , 15^1 , and 23^1 LIF bands; optimized geometries of the pyrrolyl and methyl radicals; and mass spectra of NMP recorded in REMPI experiments.

ACKNOWLEDGMENTS

We gratefully acknowledge the EPSRC for funding (Grant No. EP/L021366/1). The EPSRC and the University of Nottingham are thanked for studentships to D.J.K. and A.R.D. In addition, Warren Lawrance (Flinders University) is thanked for useful conversations.

DATA AVAILABILITY

The data that support the findings of this study are available from the corresponding author upon reasonable request.

REFERENCES

- V. Bhardwaj, D. Gumber, V. Abbot, S. Dhiman, and P. Sharma, *RSC Adv.* **5**, 15233 (2015).
- S. Chavda, K. Mulder, T. Brown, H. Mackay, B. Babu, L. Westrate, A. Ferguson, S. C. Lin, K. Kiakos, J. P. Ramos, M. Munde, W. D. Wilson, J. A. Hartley, and M. Lee, *Med. Chem.* **6**, 150 (2010).
- C. A. Downes and S. C. Marinescu, *ChemSusChem* **10**, 4374 (2017).
- Y. Fu, X. Cheng, J. Zhao, T. Kong, C. Cui, and X. Zhang, *Polym. J.* **44**, 1048 (2012).
- A. G. Sage, M. G. D. Nix, and M. N. R. Ashfold, *Chem. Phys.* **347**, 300 (2008).
- C.-M. Tseng, Y. T. Lee, and C.-K. Ni, *J. Phys. Chem. A* **113**, 3881 (2009).
- L. Blancafort, V. Ovejjas, R. Montero, M. Fernández-Fernández, and A. Longarte, *J. Phys. Chem. Lett.* **7**, 1231 (2016).
- G. Piani, L. Rubio-Lago, M. A. Collier, T. N. Kitsopoulos, and M. Becucci, *J. Phys. Chem. A* **113**, 14554 (2009).
- G. Wu, S. P. Neville, O. Schalk, T. Sekikawa, M. N. R. Ashfold, G. A. Worth, and A. Stolow, *J. Chem. Phys.* **144**, 014309 (2016).
- T. Geng, O. Schalk, T. Hansson, and R. D. Thomas, *J. Chem. Phys.* **146**, 144307 (2017).
- K. C. Woo and S. K. Kim, *Phys. Chem. Chem. Phys.* **21**, 14387 (2019).
- G. Wu, S. P. Neville, O. Schalk, T. Sekikawa, M. N. R. Ashfold, G. A. Worth, and A. Stolow, *J. Chem. Phys.* **142**, 074302 (2015), and references therein.
- G. Milazzo, *Gazz. Chim. Ital.* **74**, 152 (1944).
- R. McDiarmid and X. Xing, *J. Chem. Phys.* **105**, 867 (1996).
- C. D. Cooper, A. D. Williamson, J. C. Miller, and R. N. Compton, *J. Chem. Phys.* **73**, 1527 (1980).
- J. G. Philis, *Chem. Phys. Lett.* **353**, 84 (2002).
- J. G. Philis, *J. Mol. Struct.* **651–653**, 567 (2003).
- N. Biswas, S. Wategaonkar, and J. G. Philis, *Chem. Phys.* **293**, 99 (2003).

- ¹⁹N. Kanamaru, *J. Mol. Struct.: THEOCHEM* **686**, 15 (2004).
- ²⁰A. R. Davies, D. J. Kemp, and T. G. Wright, *Chem. Phys. Lett.* **763**, 138227 (2021).
- ²¹M. J. Paterson and D. Townsend, *Int. Rev. Phys. Chem.* **39**, 517 (2020).
- ²²M. N. R. Ashfold, S. G. Clement, J. D. Howe, and C. M. Western, *J. Chem. Soc., Faraday Trans.* **89**, 1153 (1993).
- ²³D. W. Scott, *J. Mol. Spectrosc.* **37**, 77 (1971).
- ²⁴T. J. Dines, L. D. Macgregor, and C. H. Rochester, *J. Colloid Interface Sci.* **245**, 221 (2002).
- ²⁵K. B. Beć, R. Wieczorek, B. Łydzba-Kopczyńska, and J. P. Hawranek, *Acta Phys. Pol., A* **124**, 115 (2013).
- ²⁶V. L. Ayles, C. J. Hammond, D. E. Bergeron, O. J. Richards, and T. G. Wright, *J. Chem. Phys.* **126**, 244304 (2007).
- ²⁷A. M. Gardner, W. D. Tuttle, L. E. Whalley, and T. G. Wright, *Chem. Sci.* **9**, 2270 (2018).
- ²⁸N. J. Reilly, T. W. Schmidt, and S. H. Kable, *J. Phys. Chem. A* **110**, 12355 (2006).
- ²⁹J. R. Gascooke and W. D. Lawrance, *Eur. Phys. J. D* **71**, 287 (2017).
- ³⁰P. R. Bunker and P. Jensen, *Molecular Symmetry and Spectroscopy*, 2nd ed. (NRCC, Ottawa, Canada, 1998).
- ³¹A. L. Sobolewski and W. Domcke, *Chem. Phys.* **259**, 281 (2000).
- ³²A. L. Sobolewski, W. Domcke, C. Dedonder-Lardeux, and C. Jouvet, *Phys. Chem. Chem. Phys.* **4**, 1093 (2002).
- ³³A. R. Davies, D. J. Kemp, and T. G. Wright, *J. Mol. Spectrosc.* **376**, 111410 (2021).
- ³⁴A. M. Gardner and T. G. Wright, *J. Chem. Phys.* **135**, 114305 (2011).
- ³⁵A. Andrejeva, A. M. Gardner, W. D. Tuttle, and T. G. Wright, *J. Mol. Spectrosc.* **321**, 28 (2016).
- ³⁶W. D. Tuttle, A. M. Gardner, A. Andrejeva, D. J. Kemp, J. C. A. Wakefield, and T. G. Wright, *J. Mol. Spectrosc.* **344**, 46 (2018).
- ³⁷D. J. Kemp, W. D. Tuttle, F. M. S. Jones, A. M. Gardner, A. Andrejeva, J. C. A. Wakefield, and T. G. Wright, *J. Mol. Spectrosc.* **346**, 46 (2018).
- ³⁸G. Herzberg, *Molecular Spectra and Molecular Structure: III. Electronic Spectra of Polyatomic Molecules* (Krieger, Malabar, 1991).
- ³⁹A. E. W. Knight, C. S. Parmenter, and M. W. Schuyler, *J. Am. Chem. Soc.* **97**, 1993 (1975).
- ⁴⁰A. E. W. Knight, C. S. Parmenter, and M. W. Schuyler, *J. Am. Chem. Soc.* **97**, 2005 (1975).
- ⁴¹J. Li, X. Y. Li, C. Y. Zhu, and S. H. Lin, *Phys. Chem. Chem. Phys.* **12**, 14967 (2010).
- ⁴²A. R. Davies and T. G. Wright, "Unusual photoionization behavior in N-methylpyrrole" (unpublished).
- ⁴³A. M. Gardner, L. E. Whalley, D. J. Kemp, W. D. Tuttle, and T. G. Wright, *J. Chem. Phys.* **151**, 154302 (2019).
- ⁴⁴A. D. Baker, D. Betteridge, N. R. Kemp, and R. E. Kirby, *Anal. Chem.* **42**, 1064 (1970).
- ⁴⁵G. J. Rathbone, E. D. Poliakoff, J. D. Bozek, and R. R. Lucchese, *Can. J. Chem.* **82**, 1043 (2004).
- ⁴⁶D. J. Kemp, A. M. Gardner, W. D. Tuttle, J. Midgley, K. L. Reid, and T. G. Wright, *J. Chem. Phys.* **149**, 094301 (2018).
- ⁴⁷A. J. Gianola, T. Ichino, R. L. Hoenigman, S. Kato, V. M. Bierbaum, and W. C. Lineberger, *J. Phys. Chem. A* **108**, 10326 (2004).
- ⁴⁸G. Herzberg and J. Shoosmith, *Can. J. Phys.* **34**, 523 (1956).
- ⁴⁹F. Holzmeier, I. Wagner, I. Fischer, A. Bodi, and P. Hemberger, *J. Phys. Chem. A* **120**, 4702 (2016).
- ⁵⁰A. M. Schulenburg, C. Alcaraz, G. Grassi, and F. Merkt, *J. Chem. Phys.* **125**, 104310 (2006).
- ⁵¹D. V. Makhov and D. V. Shalashilin, *J. Chem. Phys.* **154**, 104199 (2021).
- ⁵²D. J. Kemp, W. D. Tuttle, A. M. Gardner, L. E. Whalley, and T. G. Wright, *J. Chem. Phys.* **151**, 064308 (2019).
- ⁵³W. D. Tuttle, A. M. Gardner, L. E. Whalley, D. J. Kemp, and T. G. Wright, *Phys. Chem. Chem. Phys.* **21**, 14133 (2019).
- ⁵⁴A. R. Davies, D. J. Kemp, and T. G. Wright, *AIP Adv.* **10**, 125206 (2020).